UNIVERSIDADE DE SÃO PAULO
ESCOLA POLITÉCNICA
DEPARTAMENTO DE ENGENHARIA METALÚRGICA E DE MATERIAIS

ADRIÀ GALLIFA TERRICABRAS

Mechanical behaviour and microstructure of duplex stainless steels

São Paulo
2015

ADRIÀ GALLIFA TERRICABRAS

Mechanical behaviour and microstructure of duplex stainless steels

Monografia apresentada à Escola Politécnica da USP como parte dos requisitos de aprovação na disciplina PMT2596 – Trabalho de Formatura II

Orientador: Prof. Dr. Cláudio G. Schön

São Paulo

2015

Acknowledgements

To my friend Eddy, for the hours we spent together in this project and for its unconditional willingness to always help, not only for the work at the laboratory but also during my integration in Brazil.

To Professor Cláudio Schoen (Department of Metallurgical and Materials Engineering, Escola Politécnica da USP), for this opportunity, for his orientation and advices and for his patience in all moments. For his determination to solve problems.

To Márcia and Breno for their help and open hand along the project.

To Ms. Jamart, Ms. Biette and Ms. Keller of EEIGM and to Ms. Regina do Nascimento and Professor Fernando Landgraf of Escola Politécnica, for allowing the realisation of this "Trabalho de Formatura" and for their help in the bureaucratic and administrative procedures for the exchange period.

To Prof. Dr. Sérgio Duarte Brandi (Department of Metallurgical and Materials Engineering, Escola Politécnica da USP) and to Acesita – APERAM South America (represented by Dr. Tarcísio Reis de Oliveira) for the samples employed in the present investigation.

To Livio and Rafael, technicians of the metallurgy laboratory, for their orientation and help, always with a smile. To the technician of water jet cut workshop, George, of PMI (Minas e Petróleo) for his collaboration in the cutting of tensile test specimens. Also to all the people in PMT (Metalúrgica e Materiais) that in one form or another have helped in some part of the project.

To my dear Mònica, for supporting me in every moment, for her patience and love.

To my parents Mari, Quim and to my sister Carla, for inspiring and supporting me always, for trusting in me. To all the friends that are always there.

Abstract

GALLIFA, A. **Mechanical behaviour and microstructure of duplex stainless steels**. Monografia (Trabalho de formatura). Departamento de Engenharia Metalúrgica e de Materiais, Escola Politécnica, Universidade de São Paulo, São Paulo, 2015.

Rolling plate specimens of different thicknesses of duplex stainless steel UNS S32304 and a cylindrical extruded specimen of super duplex stainless steel UNS S32750 have been used to investigate the mechanical behaviour of this biphasic materials. The study has been carried out performing metallographic analysis to as-received as well as to after-deformed specimens in tensile tests. Microstructure change in the necking region, behaviour of deformed austenite and ferrite phases and influence of texture anisotropy in the plastic deformation have been studied qualitatively. Hardness of both austenite and ferrite phases, strain ratio at fracture region and macroscopic mechanical properties of these duplex stainless steels have been studied quantitatively.

Keywords: duplex, stainless steels, mechanical behaviour, duplex microstructure, metallography.

Table of contents

List of Figures

List of Tables

List of abbreviations

DSS - Duplex Stainless Steels

BCC – Body Centered Cubic

FCC – Face Centered Cubic

SEM – Scanning Electron Microscope

SCC – Stress Corrosion Cracking

1. Introduction

Duplex stainless steels are two-phase materials with similar or better corrosion resistance than the best austenitic steel grades and present superior mechanical strength.

The first wrought DSS were produced in Sweden in 1930 and were used in sulphide paper industry. Duplex Castings were produced in Finland in 1936 and a patent was developed in France in 1936. During the early 70s there were two main factors that improved duplexes development and use. The first one was the increase in Nickel price that turned austenitic grades more expensive, in combination with increasing demand of good corrosion materials for offshore oil exploitations. Second the improve in steel production techniques with new techniques like vacuum and argon oxygen decarburisation (VOD and AOD).
The introduction of continuous casting in stainless steel and afterwards the addition of Nitrogen to improve welding properties lead to the second generation of DSS that we use nowadays [Alvarez-Armas, 2008].

The mechanical properties of these biphasic materials depend strongly on alloy element composition and on thermomechanical fabrication process. The first aspect proportionate the material different strengthening mechanisms like solid solution hardening and interstitial solution hardening, and the second one, mainly by cold working in extruded or rolling sheet samples, proportionate an anisotropic microstructure, or "texture", to duplex stainless steels.
Since DSS present this anisotropic configuration, the mechanical behaviour will be influenced for this effect, making it more complex to understand than for the well-known isotropic materials.
A better understanding of the mechanical behaviour of duplexes can lead to improvement in their properties and their manufacturing process. In the present study, different methods, both qualitative and quantitative will be used to better comprehend some aspects of DSS mechanical behaviour.

2. Aim of the project

The aim of this project is to better understand duplex stainless steels mechanical behaviour, both macroscopically (through tensile tests) and microscopically; mainly observing and comparing the non-deformed microstructure of DSS with the deformed one, regarding the role that austenite and ferrite phases and the crystallographic texture play during plastic yielding and fracture mechanism.

Mechanical behaviour dependency in function of rolling plate thickness and orientation of the ferrite and austenite lamellas with respect to the applied load are also object of study.

3. Review of the literature

3.1. Duplex Stainless Steels

Stainless steels are iron-base alloys containing at least 10.5% Cr. Few stainless steels contain more than 30% Cr or less than 50% Fe. They achieve their anti-corrosion characteristics through the formation of transparent and adherent chromium-rich oxide surface film. This film form at the surface of the steel and heals itself in the presence of oxygen in case of cracking. Other alloy elements are added to improve different specific characteristics, this includes nickel, molybdenum, copper, titanium, aluminium, silicon, niobium, nitrogen, sulphur, and selenium. [ASM International, 1990].

Duplex stainless steels (abbreviated as DSS hereafter) have a duplex microstructure consisting of (BCC) ferrite and (FCC) austenite. [Hornbogen, 1984] defines a duplex microstructure like a biphasic material with approximately equal number of grain boundaries alpha / alpha and beta / beta, whose sum is similar to the number of alpha / beta interfaces. Moreover, the volume fraction of both phases should be approximately 50%. The exact amount of each phase is a function of composition and heat treatment. [ASM International, 1990].

DSS structure could be considered a composite. Following the definition according to [Jones, 1998] a composite can be classified as:
(1) Fibrous composite, what consists of continuous or discontinuous fibres in a matrix.
(2) Laminated composite materials, which consist of layers of various phases.
(3) Particulate composite materials, which are composed of isolated particles in a matrix.
(4) Combinations of some or all of the first three types.
We could consider a duplex stainless steel as a hybrid composite material between composite type 1 (Fibrous composite), composite type 2 (Laminated composite) and composite type 3 (Particulate composite).

The generalized corrosion resistance of duplex stainless steels is similar to that of austenitic stainless steels with equivalent alloying contents, however, they possess good toughness, yield strengths two to three higher than those of type 304 or 316 stainless steels, and improved

resistance to stress-corrosion cracking (SCC)[1] compared with their austenitic counterparts. Fracture toughness of duplex stainless steels is intermediate between that of austenitic and ferritic stainless steels. [ASM International, 1990].

First-generation duplex stainless steels have been in use for many years. The need for improvement in the weldability as well as pitting[2] and SCC corrosion resistance of these alloys resulted in the second-generation alloys, which are characterized by the addition of nitrogen as an alloying element. [ASM International, 1990].

Second-generation duplex stainless steels are formed usually by an equivolumetric mixture of ferrite and austenite. The new duplex alloys combine the good resistance to chloride SCC of the ferritic grades with the toughness and ease of fabrication of the austenitic grades. Among the second-generation duplex alloys, Alloy 2205 seems to have become the general-purpose stainless steel. [ASM International, 1990].

The two-phase alloy carbon steels constitute a new class of materials being considered as substitute for ordinary carbon steels in many applications for weight-saving purposes. [Makinde, 1986].

Chromium is a very important element for improving the resistance of steels to the majority of corrosion types, and increases also mechanical strength. Additionally, a high chromium content implies a very good solubility of N [Zucato et al., 2002].

Molybdenum improves the resistance to corrosion in chloride environments as well as in reducing acids. An excess of Mo content combined with high N content, however, can lead to the formation of intermetallic compounds, which are prejudicial since they turn the steel more fragile [Zucato et al., 2002].

Nitrogen partly increases the resistance to corrosion and partly increases the structural stability as well as the strength of the material. Moreover, high N contents improve the reformation of austenite after welding, which ensures optimal properties for welded joints [Zucato et al., 2002].

---

[1] Stress corrosion cracking (SCC) is the growth of crack formation in a corrosive environment. It can lead to unexpected sudden failure of normally ductile metals subjected to a tensile stress, especially at elevated temperatures. [ASM International, 1997]

[2] Pitting corrosion is a form of extremely localized corrosion that leads to the creation of small holes in the metal. The driving power for pitting corrosion is the depassivation of a small area, which becomes anodic while an unknown but potentially vast area becomes cathodic, leading to very localized galvanic corrosion. [ASM International, 1987].

Chromium, molybdenum and tungsten partition to ferrite, and nitrogen and nickel partition to austenite. The differences in composition, however, are relatively small with no more than 16% difference between the compositions of the two phases for any individual element [Renton, 2006].

In order to classify corrosion resistance of different duplex grades, some authors define the empirical pitting resistance equivalent number (PREw), which combines the percentage weight of chromium, molybdenum, tungsten and nitrogen to give the formula (1):

$$PREw = Cr + 3.3Mo + 1{,}65W + 16N \quad (1)$$

Duplex grades with a PREw greater than 40 are known as super-duplex. [Alvarez-Armas, 2008] In the following Table 1, the PREw number for different stainless steel grades is presented.

Table 1. Composition and PREw number for different Duplex, Austenitic and Superaustenitic Steel Grades [Alvarez-Armas, 2008].

Grade	UNS	C	Cr	Ni	Mo	W	Cu	N	PRE_{sw}
Lean Duplex	S32101	0.03	21.5	1.5	0.3	-	-	0.22	25
	S32304	0.02	23	4	0.3	-	0.3	0.10	25
Standard Duplex	S31803	0.02	22	5.5	3.0	-	-	0.17	35
	S32205		22.5	5.8	3.2	-	-	0.17	36
Superduplex	S32750	0.02	25	7	4.0	-	0.5	0.27	43
	S32760	0.03	25	7	3.5	0.6	0.5	0.25	42
Superaustenitic									
904L	N08904	0.02	20	24.5	4.2	-	1.5	0.05	35
254 SMO	S31254	0.02	20	18	6.1	-	0.7	0.20	43
Austenitic									
304L	S30400	0.02	18.2	8.1	0.3	-	-	0.07	20
316L	S21600	0.02	16.3	10.1	2.1	-	-	0.07	24
317L	S31703	0.02	18.4	12.4	3.2	-	-	0.07	30

Among stainless steels, Austenitic remains the most popular grades, followed by Ferritic ones. Duplex grades production, worldwide, represent nowadays about 200kT, less than 1% of the total production. However, the production has growth of more than 100% in the latest decade due to its interesting mechanical and corrosion resistance properties. [Charles, 2007].

Most of the duplex applications concerns highly corrosion resistance properties encountered in process industry: Chemical, petrochemical, off-shore, chemical tankers, pulp and paper industry, pollution control equipment, desalination and sea-water applications. [Charles, 2007].

3.2. Formation and phases present in Duplex Stainless Steels

Lean duplex stainless steels solidify in a completely ferritic structure, afterwards austenite transformation occurs in the solid state (Figure 1). The ferrite-austenite transformation, is reversible, for that reason, a significant increase in temperature from 1050°C to 1300°C, for example, leads to a higher ferrite content. Austenite nucleates around 1300°C and grows early in the grain boundaries of ferrite and afterwards inside the ferrite grains. [Padilha and Plaut]. However, in super duplex stainless steels solidification of austenite can occur directly from the liquid.

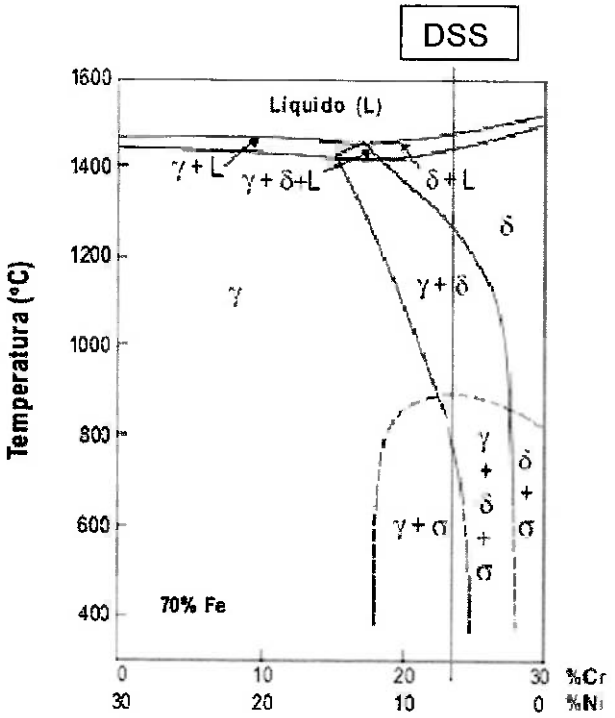

Figure 1. Pseudo binary phase diagram Fe - Cr - Ni obtained from a ternary diagram cut at 70% Fe [3]. The line below "DSS" marks approximately the compositions where duplex stainless steels are present. Adapted from [American Society for Metals, 1973].

As stated above, the two main phases present in DSS, and responsible of its good macroscopic mechanical properties are austenite and ferrite. The ideal balance for modern duplexes varies among fabricants, but a volume fraction from 45% to 60% can be expected to

[3] The aim of the figure is to show qualitatively the shape of the Fe – Ni – Cr diagram in duplex steels. However, for modern duplex steels, pseudo binary phase diagrams are no more presented with a cut at 70% Fe, but at 60% due to increasing alloy content.

have the most optimal properties. Mechanical aspects are further developed in point *3.4. Mechanics of duplex stainless Steels.*

When DSS are exposed to temperatures ranging from 300 to 500 °C, α' phase formation can occur, and at temperatures ranging from 500 to 1000 °C, phase transformations such as the sigma phase formation, chromium nitrides and carbides precipitation are favoured.
The occurrence of these phases can often cause loss of toughness and a decrease in corrosion resistance. The sigma phase presents the fastest kinetics in the range of temperatures reached during welding or thermo-mechanical processing [Zucato et al., 2002].

The different possible phases present in DSS are shown in the following Table 2:

Table 2. Secondary phases present in DSS. Lattice constants in Angstroms [Å]. Adapted from [Nickel Development Institute, 2000].

Phase	Symbol	Type	Formula	Temperature Range	Structure	Lattice Constants
chromium carbide	-	M_7C_3	$(Cr,Fe,Mo)_7C_3$	950-1050°C	orthorhombic	a=4.52, b=6.99, c=12.11
chromium carbide	-	$M_{23}C_6$	$(Cr,Fe,Mo)_{23}C_6$	600-950°C	cubic	a=10.57-10.68
chromium carbide	-	M_6C	$(Cr,Fe,Mo,Cb)_6C$	700-950°C	cubic	a= 10.93-11.28
chromium nitride	-	M_2N	$(Cr,Fe)_2N$	650-950°C	hexagonal	a=2.77, c=4.46
chromium nitride	-	MN	CrN	-	cubic	-
Fe-Mo nitride	-	M_2N	$Fe_2Mo_2N_4$	550-600°C	-	a = 6.47
Sigma	σ	AB	(Fe,Cr,Mo,Ni)	550-1050°C	tetragonal	a=8.79, c=4.54
Chi	χ	$A_{48}B_{10}$	$Fe_{36}Cr_{12}Mo_{10}$ $(FeNi)_{36}Cr_{18}(TiMo)_4$	600-900°C	cubic	a=8.86-8.92
Alpha prime	α'	-	CrFe(Cr 61-83%)	350-550°C	cubic	a=2.877
Laves	η	A_2B	$(FeCr)_2(Mo,Nb,Ti,Si)$	550-900°C	hexagonal	a=4.73-4.82, c=7.26-7.85
R	R	-	(Fe,Mo,Cr,Ni)	550-650°C	rhombohedral	a=10.903, c=19.347
Tau	τ	-	-	550-650°C	orthorhombic	a=4.05, b=4.84, c=2.86

An embrittlement near 475°C is caused by alpha prime formation, which is traduced in an increase of hardness of the ferrite phase. A significant 475°C embrittlement appears for more than 10 h of treatment in UNS S31803 for example, according to [Brandi, 1992].

Sigma phase consumes chromium and molybdenum of the duplex matrix. In consequence, the material suffers a globally loss in corrosion resistance.

Apart from chemical composition, there are other factors influencing sigma phase precipitation, like grain size: the smaller the grain size, the more tendency to form sigma phase. Sigma phase is more likely to form in high energy zones like grain boundaries or interphases. [Zucato et al., 2002]

The precipitation of other phases such as Carbides $M_{23}C_6$ and Nitrides (CrN and Cr_2N) can also occur in DSS, presenting the same negative effects as sigma phase and forming as well in the grain boundaries or interphases. [Zucato et al., 2002].

3.3. Mechanics of duplex stainless steels

The main reason for the high strength of DSS is the fine grain size, that is achieved because the ferrite and austenite phases prevent each other from grain growing. In consequence, there are multiple interphase boundaries locking the dislocations movement, which is traduced at a macroscopic level as a strengthening in the material. [Sandvik, 1994].

The combination of properties of both austenite and ferrite plays a key role in the macroscopic mechanical properties of DSS. In the following Table 3. some mechanical properties of austenite and ferrite are presented:

Table 3. Some mechanical properties of austenite and ferrite. [?, Apud Hirano, 2006].

Property	Ferrite	Austenite
Slip systems	48	12
Stacking fault energy	Higher	Lower
Slip with deviation	Easier	More difficult
Dislocation distribution	less uniform	more uniform
Work Hardening	Lower	Higher
Peierls-Nabarro Stress	Higher	Lower
Yield Strength	Lower	Higher
Tensile Strength	Lower	Higher

Atoms in the ferrite are organized in a BCC primary lattice structure, less close-packed than in FCC (austenite) and present considerably more slip systems to be activated. [Sandvik, 1994]. This last fact means, in principle, that BCC structures should be more ductile than FCC ones. In the Figure 2. below the two lattice structures can be compared:

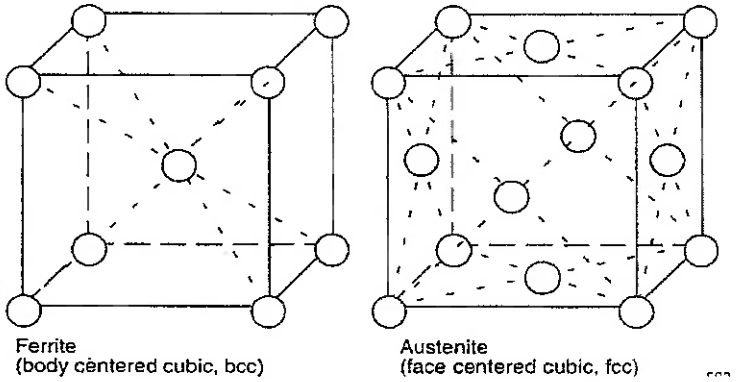

Figure 2. Ferrite (left) and austenite (right) primary lattice structures. [Frodigh. (Sandvik) 1994]

Peierl's stress (equivalent to "lattice friction") is minimized by small Burgers vector b, and large lattice spacing a. Therefore, dislocation motion in cubic crystals tends to occur on closed packed planes in which the magnitudes of Burger's vectors, b, are minimized and the vertical lattice spacing, a, are maximized. Since lattice friction stresses are minimized on such planes, dislocation motion is most likely to occur on closed packed planes along close packed directions. [Soboyejo, 2002].

Slip in Face Centered Cubic structures (FCC): close packed planes in FCC materials are of the {1 1 1} type. The closed packed directions correspond to (1 1 0) directions along the sides of {1 1 1} planes. Since there are four slip planes with three slip directions each one, this indicates there are 12 possible {1 1 1}(1 1 0) slip systems. [Soboyejo, 2002].

Slip in Body Centered Cubic structures (BCC): in the case of BCC, there are no close-packed planes, although the {1 0 1} planes are the closest packed. The close pack directions in BCC are the (1 1 1) directions, therefore slip is most likely to occur in {1 0 1} planes along (1 1 1) directions. However slip may also occur in {1 1 0}, {1 1 2} and {1 2 3} planes also along (1 1 1) directions. Therefore, the total number of possible slip systems is 48. Nevertheless, the large number of possible slip systems in BCC crystals do not necessarily promote improved ductility since the lattice fraction (Peierls-Nabarro) stresses are generall higher in BCC structures. [Soboyejo, 2002].

Due to this contrary effect - for example in the ferrite: it has more slip systems but no close-packed planes, so it has higher lattice friction - in terms of defining which phase will deform easily, it is expected that depending on different parameters (like work hardening amount or alloying element content), ferrite can be harder than austenite or vice versa.

According to [?, Apud Hirano, 2006], what defines which phase is the most ductile depends on Nitrogen content: if its content is higher than 0,13%, austenite will be harder, on the contrary, it will be the ferrite. That is because Nitrogen tends to harden the austenite by interstitial hardening. As it can be seen also in the Table 3, austenite is more susceptible to harden by work hardening. Consequently, high N content and cold worked duplex stainless steels are expected to have a harder austenite and a more ductile ferrite.

3.3.1. Plastic Deformation

During plastic deformation of a two phase material, the flow behaviour of the constituent phases differs significantly compared to their single phase plastic properties, and the macroscopic plastic behaviour is often anisotropic [Moverare 2002].

Ferrite is more likely to deform plastically through screw dislocations, while austenite can deform both by edge or by screw dislocations. Therefore this last one presents a mixed dislocation behaviour. In the image below a representation of a srew, an edge dislocation and a mix dislocation (combination of the two first, with a circular dislocation line) are represented.

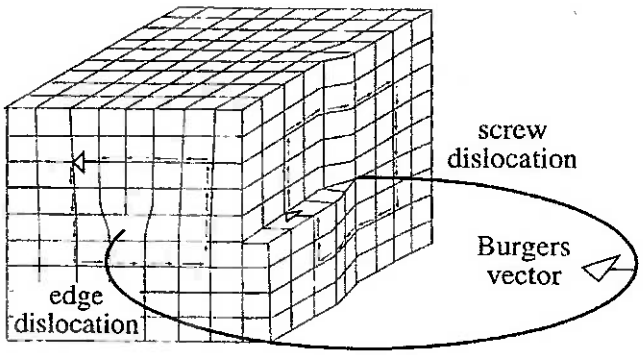

Figure 3. Shows the relationship between an edge and screw dislocation in an idealized three dimensional crystal lattice. By [Passchier and Trouw, 2005].

The movement of dislocations can stop at the surface of the material, at a grain boundary, at a precipitate or onto another defect. During dislocations sliding, blocks of material can move one respect to another along the crystallographic slip planes.

When this happens, atoms move an integer number of atomic distances and along these planes, producing a step on the surface. These steps when observed in an optical microscope (Figure. 4) appear as lines, called slip bands that correspond to each active system.

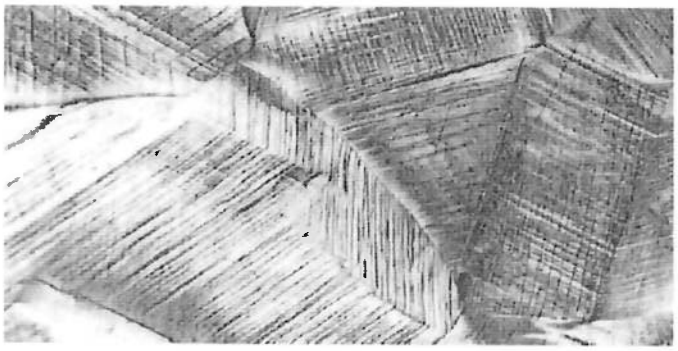

Figure 4. Slip bands on the surface of a polished deformed polycristalline sample (Callister, 2002).

An alternative mode of permanent deformation in metals, without dislocation movement, is twinning, for example in austenite. Twinning refers to the atomic arrangement within a crystal where a region of the crystal takes on a different crystallographic axis orientation from the rest of the crystal; the structures on either side of the boundary (between the two different orientations) are crystallographically identical as if they are reflections across a mirror plane. The boundary is called a twinning plane. The portion having a lattice orientation that is different from the original orientation is called a twin. Twinning can occur in a metal either during solidification as shown in or as a result of being stressed to a state of plastic deformation (Figure 5) [Kenneth, 2012].

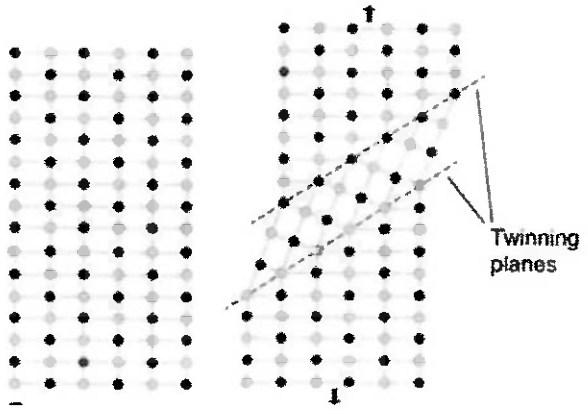

Figure 5. A lattice structure before and after plastic deformation of a metal by twinning under tension. Note that the shape of the object has changed but the relative position of the atoms remains unchanged. Also note that the atoms on either side of the twinning plane have a mirror relationship. Adapted from [Kenneth, 2012].

The interphases encountered along the material can be low angle or high angle grain boundaries, free surfaces, stacking faults, twinning boundaries, etc. They separate crystalline regions with different crystallographic orientation and they can be usually described as surface defects.
In the specific case of DSS, not just the interphases between α/α and γ/γ but also the interphase α/γ have an essential importance in his behaviour during plastic deformation.
The grain boundaries have an energy per surface unit associated, in other words surface tension. This energy is practically a constant in a material [Bevitori, 2010].

When a DSS is under a load, since it is a duplex phase material, firslty both phases start to deform elastically and at some point the most ductile phase starts to defrom plastically. Afterwards the two phases deform plastically. [?, Apud Hirano, 2006].

3.3.2. Strengthening Mechanisms

There are several methods to strengthen metals. They all act in the same fundamental way, which is to prevent the dislocations from moving. Is the dislocations movement that make the material easy to deform, and if they can not move the material becomes stronger. This can be achieved by 4 main ways [Sandvik, 1994]:

1. Reducing grain size (According to Hall-Petch relation).
2. Adding elements that go into substitutional solutions in the lattice.
3. Adding elements that go into interstitial solutions in the lattice.
4. Cold deformation hardening.

The grain size is small because the two phases prevent each other from growing. The grain size hardening mechanism is very beneficial from DSS because it will increase both strength and toughness. The rest of hardening mechanisms do not have this double effect and are as well effective in austenitic grades and duplexes. [Sandvik, 1994].

The substitutional solution hardening acts by making more difficult to the dislocation to move because the regularity in the lattice is disturbed. The strengthening of different alloy elements will be different in each phase. For example, in DSS, Cr and Mo stabilize the ferrite phase and Ni the austenite phase. [Sandvik, 1994].

Interstitial solution hardening consists in place new atoms between interstices of the atoms of the original lattice. The way they block the dislocation movement are similar to the substitutional one, but they are more effective. In DSS Nitrogen has this effect in austenite phase. [Sandvik, 1994].

When a material is deformed at room temperature or up to approx.. 0,3 Tm[4], the microstructure becomes deformed due to cold working. During this process, most of the energy is dissipated in the workpiece as heat, but about a 10% is retained as stored energy inside the material, in form of vacancies, dislocations and stacking faults. The amount of stored energy, stacked inside the crystalline lattice, increases with the amount of deformation and lower working temperatures. During cold rolling, grains and their slip planes try to align themselves with the direction of rolling, as shown schematically in Figure 6. [ASM International, 2011].

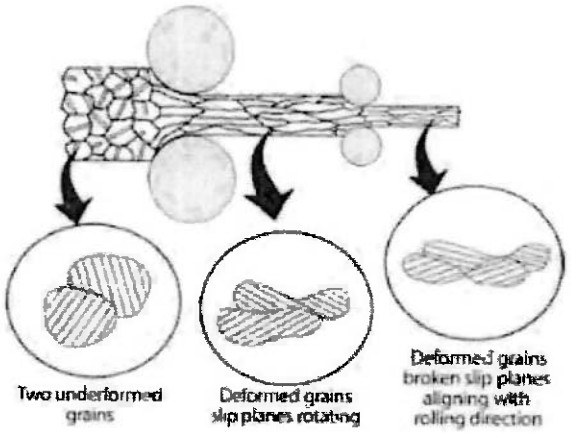

Figure 6. Scheme of grain and plane preferred orientation during cold working process. [ASM international, 2011].

Strong cold working can lead to preferred orientations (or texture, or anisotropy) in which grains become oriented along certain crystallographic planes with respect the direction of the applied stress. [ASM International, 2011].

In rolling plate samples the final texture is clear, and distinct sections of the specimen can be observed with respect to the rolling direction; in the Figure 7 below, typical anisotropic structure of DSS is presented:

[4] Tm = Melting Temperature.

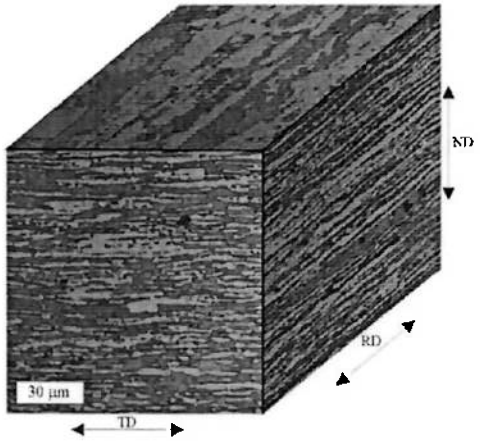

Figure 7. Schematic representation of the microstructure texture in a rolling plate sample; Rolling Direction (RD) or Longitudinal, Transverse Direction (TD) and Normal Direction (ND) [Moverare 2002].

3.3.3. Plastic behaviour due to Anisotropy

Apart from their excellent mechanical and corrosion resistance properties, two-phase steels perform poorly in sheet-forming operations. [Makinde, 1986].

Formability is related not only to strain hardening but also to various other continuum properties of a material such as anisotropy. For that reason, it is necessary to understand the interaction and influence of the anisotropic properties of the constituent phases on the final properties of resulting biphasic material. [Makinde, 1986].

In the following Figure 8, variations in the plastic strain ratio[5] (r) as function of the angle between the tensile axis and the rolling direction is showed:

[5] Strain ratio is defined as the ratio of the width to the thickness deformation during simple tension tests in any particular direction.

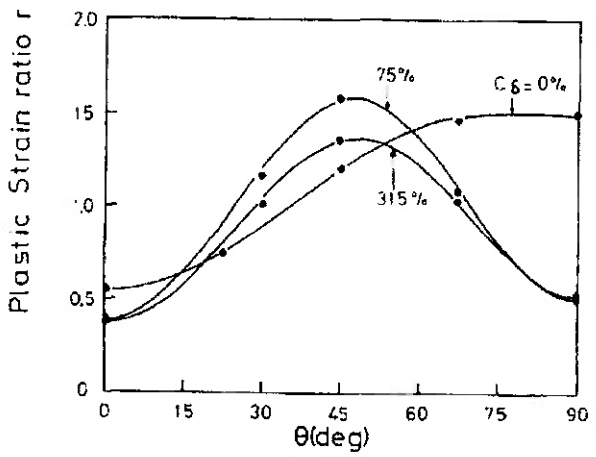

Figure 8. Variations in the plastic strain ratio (r) as function of the angle between the tensile axis and the rolling direction. Curves for 31,5 %vol, 75 %vol and 0 %vol of ferrite are presented.

From Figure 8. it can be deduced that anisotropic deformation in DSS is not only dependent on the respective orientation between rolling direction and load direction but also on the volume ratio of austenite/ferrite present in the steel.

For a state of uniaxial stress in a two-phase material, the difference between the anisotropies of the phases present gives arise to a biaxial stress state in each phase. This phenomena can be observed in the results stated for [Makinde, 1986] and presented in Figure 9 :

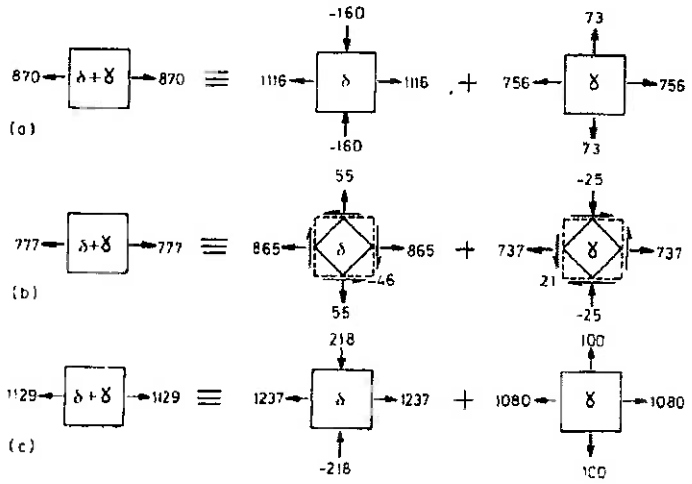

Figure 9. Schematic representation of the in situ stress state simulation in the constituent phases for simple tension tests on the duplex steel with 31,%vol ferrite: a) 0° ; b) 45° ; c) 90°. The numerical values correspond to stresses in MPa calculated at the point of maximum force on the two-phase material. [Makinde, 1986].

In the figure 9. it can be observed that a uniaxial load applied macroscopically to the material leads to a different biaxial stress in each different phase. In the first case, for example, ferrite is under a stress state composed by traction in the horizontal axis and compression in the

vertical one, while austenite is experiencing traction in both axes. This example pretends just emphasize that discontinuities in the stress state will appear in the interphase γ/α leading to micro voids formation and further decohesion of the material.

3.3.4. Fracture of ductile materials

Alloys undergo brittle fracture or ductile fracture, depending on a variety of factors, such as composition, microstructure, temperature, and strain rate. [Kenneth, 2012].

Ductile fracture in metals is a multistep mode of material failure incorporating the combination of micro void nucleation, growth and coalescence at the microscale level, according to [Ruggieri, 2004]. Early experimental studies demonstrated the key role played by micro void mechanisms on ductile failure of tensile specimens (Puttick, 1959). An increasing population of micro voids is forming inside the material as long as the neck is forming during a tensile test as it can be seen in Figure 10.

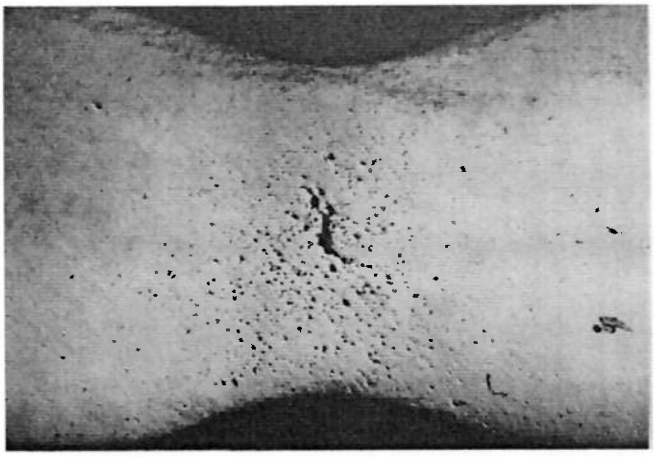

Figure 10. Section through the neck of a tensile specimen of copper. Cavities coalescing in the neck before fracture. Load direction: horizontal. [K.E. Puttick, 1958].

The micro voids that act as sites of fracture initiation can arise from multiple causes, including an accumulation of dislocations or strain boundaries between two different microstructural phases, [Kenneth, 2012] most often they concentrate in the centre of the neck region. Under increased deformation, these micro voids grow until localized plastic flow and necking of the ligament between adjacent micro voids (coalescence of micro voids) create a continuous fracture path (See Figure 11.) (most often assisted by the rapid growth and coalescence of secondary micro voids). Upon further deformation, this internal crack progresses until sufficient

loss of cross sectional area leads to final failure of the specimen by a plastic collapse mechanism of the remaining ligament [Ruggieri, 2004].

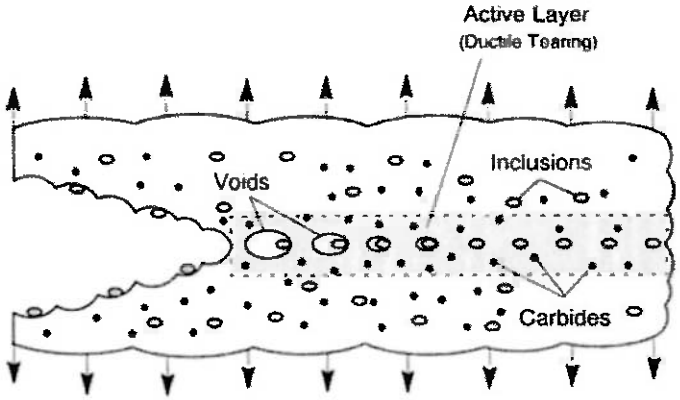

Figure 11. Phenomenological modeling of ductile fracture. Schematic path of a growing crack in a ductile material. [Ruggieri, 2004]

4. Methods

- In the first part of the project the microstructure of different as-received materials have been analysed using an optical microscope (OLYMPUS-BX60M). Specifically, four duplex stainless steel UNS S32304 rolling plate samples (with different plate thicknesses each one) and an extruded cylindrical super duplex stainless steel UNS S32750 sample have been investigated.

  Metallographic analysis have been carried out in the longitudinal, transverse and superficial direction sections (with respect to the rolling direction) for the rolling plates, and in the longitudinal and transverse directions for the cylindrical sample. This early studies serve to establish a reference for the as-received specimen microstructures in order to compare it afterwards with some deformed specimens.

- In a second part, different tensile tests have been performed. Concerning the cylindrical sample, one specimen has been tested (load in the cylinder's axis direction) until fracture.
  Regarding the rolling plates, 2 tensile tests have been performed for each plate type: one tensile test in which the tested specimen has been cut parallel to the rolling direction and one in which the specimen has been cut in the transverse direction. In all cases the tests have been as well until fracture.
  The deformed tested specimens have been prepared in order to do metallographic studies, again, using the optical microscope.
  Particular attention has been paid in the observation of the necking part of the deformed specimens, where a high heterogeneous plastic deformation is produced before macroscopic fracture of the specimens occurs.
  Different phenomena derived from the plastic deformation of duplex stainless steels have been analysed through these metallographic analysis after tensile tests.

Finally, some other experiences have been carried out to complement the early studies:

- The fractured regions of the ruptured specimens have been photographed using SEM. (FEI-Inspect F50).

- Study the hardness of both phases austenite and ferrite through Vickers Hardness test of a different rolling plate sample and also for the cylindrical sample.

4.1. Material

As-received material:

Four rolling plate UNS S32304 samples (with different thicknesses) provided by the company Aperam S.A. have been analysed. The Table 4. below shows up every plate thickness and its corresponding chemical composition:

Table 4. Chemical composition of as-received DSS rolling plates UNS S32304.

Thickness/Comp.	C [%w.]	Cr [%w.]	Ni [%w.]	Mo [%w.]	Cu [%w.]	N [%w.]	S [%w.]	W [%w.]
3,0 mm	0,0096	22,1646	3,51	0,357	0,431	0,1162	0,0006	0,0118
5,3 mm	0,0193	22,2597	3,8019	0,246	0,4361	0,1070	0,0001	0,0124
6,3 mm	0,0192	22,346	3,727	0,2386	0,4623	0,1043	0,0007	0,0106
10,4 mm	0,0178	22,558	3,5721	0,2594	0,4244	0,1206	0,0003	0,0102

UNS S32750 specimens have been obtained from an extruded cylindrical cross-section bar of 25mm diameter.

Table 5. General chemical composition of UNS S32750 super DSS. Based on [Sandvik 2507].

C [%w.]	Cr [%w.]	Ni [%w.]	Mo [%w.]	Cu [%w.]	N [%w.]	S [%w.]	Mn [%w.]
0,03	25	7	4	≤ 0,5	0,30	≤ 0,015	≤ 1,2

As it can be seen, UNS S32750 has basically a higher concentration of all alloying elements than UNS S32304. That fact will provide to the super DSS improved mechanical and corrosion properties but also a higher price.

4.2. Metallography

The process used to prepare the specimens in order to perform the metallography has been divided in the following steps:

4.2.1. Sectioning

The rolling as-received plates were cut by the supplier with a metal shear. In the laboratory, to produce the different samples for the metallographic study, a power hacksaw, a band saw or an abrasive cut-off wheel have been used. Such tools can produce substantial deformation on the microstructure in the cut edges, according to [Vander 2004]. For that reason observations with the optical microscope have been performed, when possible in the centre of the specimen surface or, at least, at a prudent distance from the edges, from 1mm approx.

4.2.2. Mounting

The cut samples have been mounted in a mounting machine, with the following parameters: Total time: 15 min., Maximum Temperature: 175º, Maximum Pressure: 13,7 MPa (2000 psi), Polymer type: Thermoset, Bakelite.

4.2.3. Grinding

Grinding has been performed by hand using P180, P320, P400, P600, and P1000 or P1200 grit water-cooled silicon carbide (SiC) papers. Speeds of 240 to 300 rpm and moderate firm pressure has been applied. The specimens have been rotated 90° between each step, according to [Vander 2004].

4.2.4. Polishing

The grinded specimens have been polished at 6µm, 3µm and 1µm diamond paste with napped polishing cloths. Same speeds as for grinding low-moderate firm pressure have been applied.

4.2.5. Micro etching

According to [Vander 2004] the attack of a duplex stainless steel can show optimal results with an electrolytic etching with oxalic acid:
"Popular electrolytic etch; 6 V dc. 15–30 s reveals carbides; grain boundaries revealed after 45–60 s; σ phase outlined after 6 s. Lower voltages (1–3 V dc) can be used. Dissolves carbides. Sigma strongly attacked, austenite moderately attacked, ferrite not attacked."

A solution of oxalic acid with distilled water: 100g of oxalic acid per 1L of solution has been used. Voltages between 2 and 4 Volts have been used during approximately 40 seconds. Visual control of the specimen surface has been used to prevent over-etching. While getting attacked, the surface loses progressively its mirror brightness and a yellow substance result from the removed surface of the specimen is formed.

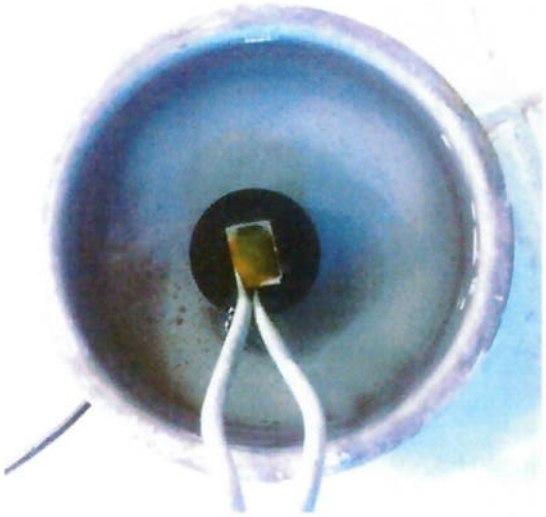

Figure 12. Yellow surface of the polished DSS during attack with oxalic acid. Top view.

4.2.6. Optical Microscope observation

Observations have been carried out at 50x, 100x, 200x, 500x and 1000x magnification for the most part of specimens. Light intensity, contrast and focus have been kept as homogeneous as possible for the whole image area, trying to avoid texture effects and allowing a clear distinction of phases in the microstructure.

After performing the metallographic preparation, different images for each specimen have been taken. Representative images form the Longitudinal, Transverse an Superficial sections for the rolling plate samples are presented in the results, as well as longitudinal and Transverse sections for the cylindrical specimen. In the following Table 6, a designation of all the as-received samples studied is presented:

Table 6. Scheme for sample designation. List of metallographic analysed specimens. Description, observed section and simplified name are presented.

Description	Observed section	Simplified Name
3mm rolling plate	Superficial	X3S
	Transversal	X3T
	Longitudinal	X3L
5,3 mm rolling plate	Superficial	X5S
	Transversal	X5T
	Longitudinal	X5L
6,3[6] mm rolling plate	Superficial	X6S
	Transversal	X6T
	Longitudinal	X6L
10 mm rolling plate	Superficial	X10S
	Transversal	X10T
	Longitudinal	X10L
Cylindrical	Transversal	CT
	Longitudinal	CL

[6] Hereafter, 6,3mm thickness rolling plate can be designed also as 6mm interchangeably. The same with 5mm for the 5,3mm thickness rolling plate sample

4.3. Tensile Tests

4.3.1. Specimens

The tensile tests have been performed to the following samples stated in Table 7:

Table 7. Description, Specimen cut orientation respect to the rolling direction and simplified name of the tested specimens.

Description	Specimen orientation	Simplified Name
10mm rolling plate	Longitudinal	X10L_fract
	Transverse	X10T_fract
6mm rolling plate	Longitudinal	X6L_fract
	Transverse	X6T_fract
Cylindrical	Longitudinal	CL_fract

The following drawings (Figure 13) have been used to cut the sheet tensile test specimens.

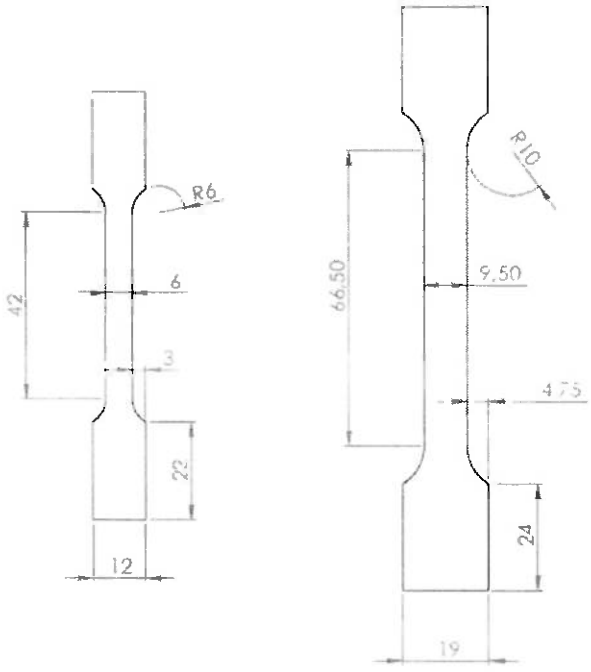

Figure 13. Dimensions of the tensile test specimens for the rolling plate samples. Each model has been used for a different rolling plate: Left 6mm thickness sheet ; Right 10mm thickness sheet.

Concerning the central part of the specimens (useful part), the criteria used for the conception of the drawings is based in the most of international tensile test norms: "the width of the central part of specimen has to be at least four times the length of the useful part." In the present study, the length has been fixed at 7 times the width.

For the 6mm and 10mm rolling plates, 2 specimens have been cut in the longitudinal direction (following the rolling direction) and 2 in the transverse direction, as it shows the Figure 14.

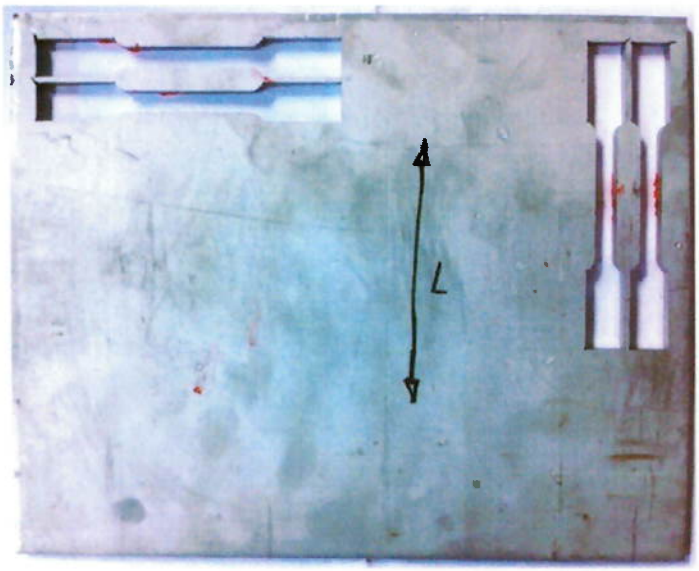

Figure 14. Rolling plate with 2 tensile test specimens cut in the rolling direction (vertical, right side) and 2 cut in the transverse direction (horizontal, upper side). The rolling direction is stated with the arrow.

The schematic representation of the lamellas respect to the load direction is presented in the following figure 15:

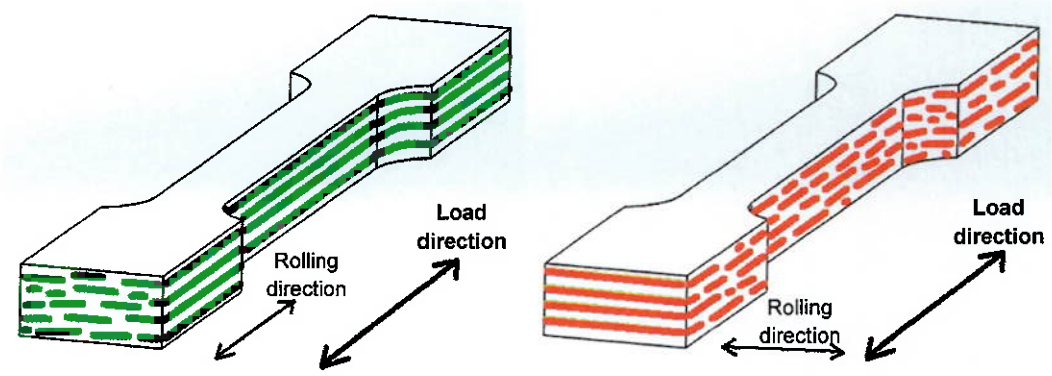

Figure 15. Schematic representation of lamella disposition in longitudinal cut specimen (left) and transverse cut specimen (right) respect to the tensile load direction.

After grinding the tensile test specimen surfaces with 100P, 220P, 400P and 600P SiC paper to avoid surface defects influence on the fracture behaviour, width and thickness in three regions of the central part of the specimen have been measured. In the following Table 8 the average initial width and initial thickness are presented. Also the initial corss section suposing it was a rectangle:

Table 8. Average Width, Thickness and cross-section area of central part of specimens before testing.

	$Width_0$(mm)	$Thick._0$(mm)	S_0(mm^2)
10mmL	9,50	10,20	96,90
10mmT	9,42	9,93	93,54
6mmL	5,95	6,22	36,99
6mmT	6,00	6,30	37,80

The following drawing has been used for cutting the cylindrical tensile test specimen.

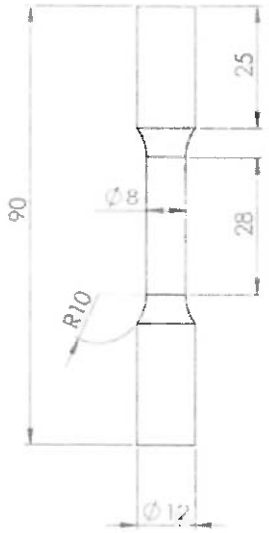

Figure 16. Cylindrical specimen dimensions.

4.3.2. Tensile test machine

MTS Landmark Servohydraulic Test machine of 250kN maximal force has been used to perform the tensile tests. Time, displacement and force have been recorded using the *MTS TestSuite Software*. The acquisition rate has been of 10 measures / second. Due to the lack of extensometer, the displacement recorded has been the one from the mobile crosshead. As the machine it is not a full rigid system, some bias can be introduced, including therefore some displacement from the machine in the total measured displacement. That could have a

significant influence in the calculation of the young Modulus (E). However, as the machine used (25 tons of maximal force) is over dimensioned respect to the maximal admissive force for the specimens (7,5 tons approx. for the 9,5mm thickness specimen) the errors in the measures are expected to be not very high.

4.3.3. Tensile Test data processing

The elements extracted from the tensile tests have been, for each specimen: Stress vs. Strain engineering curve, Young Modulus, Yield strength, Ultimate Tensile Strength (UTS), Breaking Strength, uniform Elongation (plastic elongation at neck formation) and total Elongation (plastic elongation at facture), calculed as:

Stress=F/A_0 , Where F force in N is recorded directly and A_0 initial cross section of the specimens at the central part, calculated as an average of 3 measurements of [thickness x width] as showed in the Table 8 above.

Strain= Displacement/L_0 , where displacement directly recorded by the machine and L_0 the distance inlcuding the central part of the specimen until the fixing part where the serrated wedges attach the specimen. This criteria can introduce some errors since the wider parts close to the radius of the specimens are not deforming at the same ratio as the central narrow part. However, since the present study is carried out in order to compare the behaviour of the different specimens and not to characterize precisely the mechanical properties of the specimens, this approximation will be useful.

The Young Modulus E has been extracted from the slope of the linear regression of the first Strain and Stress curve points. Values until 300 MPa of stress have been taken in account for all the curves, because until this value the curves present, apparently, a straight behaviour.

The Yield Streght has been stated at the point where Stress vs. Stress curve intersects with the straight of young Modulus (E) translated at a stress value of 0,002. Corresponding to 0,2% of plastic deformation.

Breaking Stregth: The last value of Stress curve has been taken as Fracture Stregth and the corresponding strain (after subtracting the corresponding elastic deformation → $\varepsilon_{elastic\ part} = \sigma_{Strength}/E$) has been stated as total Elongation.

Ultimate Tensile Stregth : The maximum value of Stress curve has been taken as Ultimate Stregth and the corresponding strain (after subtracting the corresponding elastic deformation → $\varepsilon_{elastic\ part'} = \sigma_{Ultimate}/E$) has been stated as uniform elongation.

4.4. Hardness

Micro hardness Vickers test has been performed to determine the hardness of the phases present in the microstructure, using *HMV - Micro Hardness Tester* equipment by SHIMADZU and the software *HMV-AD* from the same fabricant.
The equipment incorporates an optical microscope to fix the point in where the indentation is produced plus a diamond square-based pyramid indenter.
The force used has been 98,07mN (10g), the minimum permitted by the machine, that gives an indentation small enough to fit inside both ferrite and austenite grains, respectively. Therefore the hardness measure will be expressed as $HV_{0,01}$ and calculated according to equation (2), according to [ASTM E384].

$$HV = \frac{1{,}8544 \cdot F}{d^2} \quad (2)$$

F in kg, d in mm.

The software allows performing the measures of the diagonals of the indentation directly fitting de indentation rhombus inside a mobile rectangle, on the image seen by the microscope. The criteria used has been put the sides of the rectangle as close as possible to the rhombus vertices, but without touching them.

The hardness of UNS S32304 has been measured in a rolling plate sample, more specific on the 10mm thickness rolling plate, longitudinal surface (10L).
The hardness of UNS S32750 has been measured in the cylindrical sample, transverse surface (CT).

4.5. SEM

SEM INSPECT F50 has been used to take images of the fracture of after-tested specimens. The fracture necks have been cut 1cm from the fracture approximatively, and washed by ultrasound in acetone during 5 minutes, before acquiring the images with the SEM.

The tension used has been 20kV with the ETD detector and same magnifications have been used in order to compare the images taken for the different samples.

5. Results and Discussion

5.1. Austenite and ferrite identification

One important step in this project for being able to analyse further results is austenite and ferrite identification. In the optical microscope austenite appears always in brighter grey than ferrite, which is darker. Moreover, inside austenite twinning phenomena can be identified, appearing as bands formed for parallel or quasi-parallel lines inside the phase. See Figure 17.

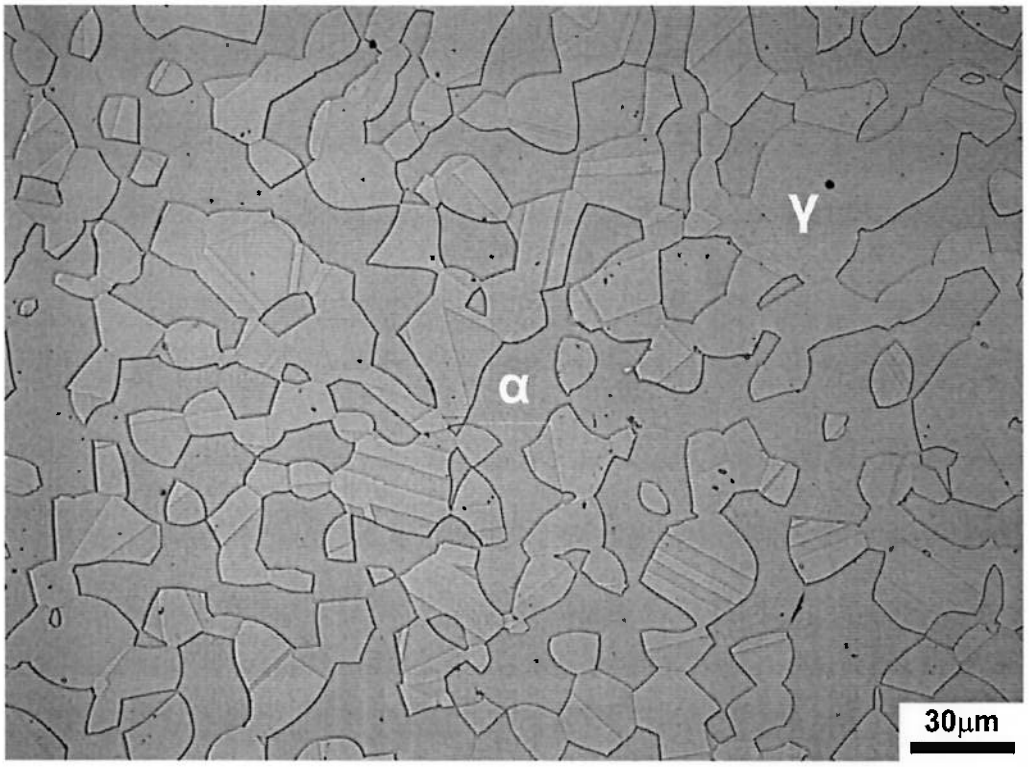

Figure 17. Austenite (bright grey) with twinning phenomena inside and ferrite (dark grey). CT sample. Magnification 500x.

5.2. Metallography of as-received samples

In this part the microstructure of different rolling plate samples according to longitudinal, transverse and superficial sections are presented in some images and discussed.

3mm thickness rolling plate

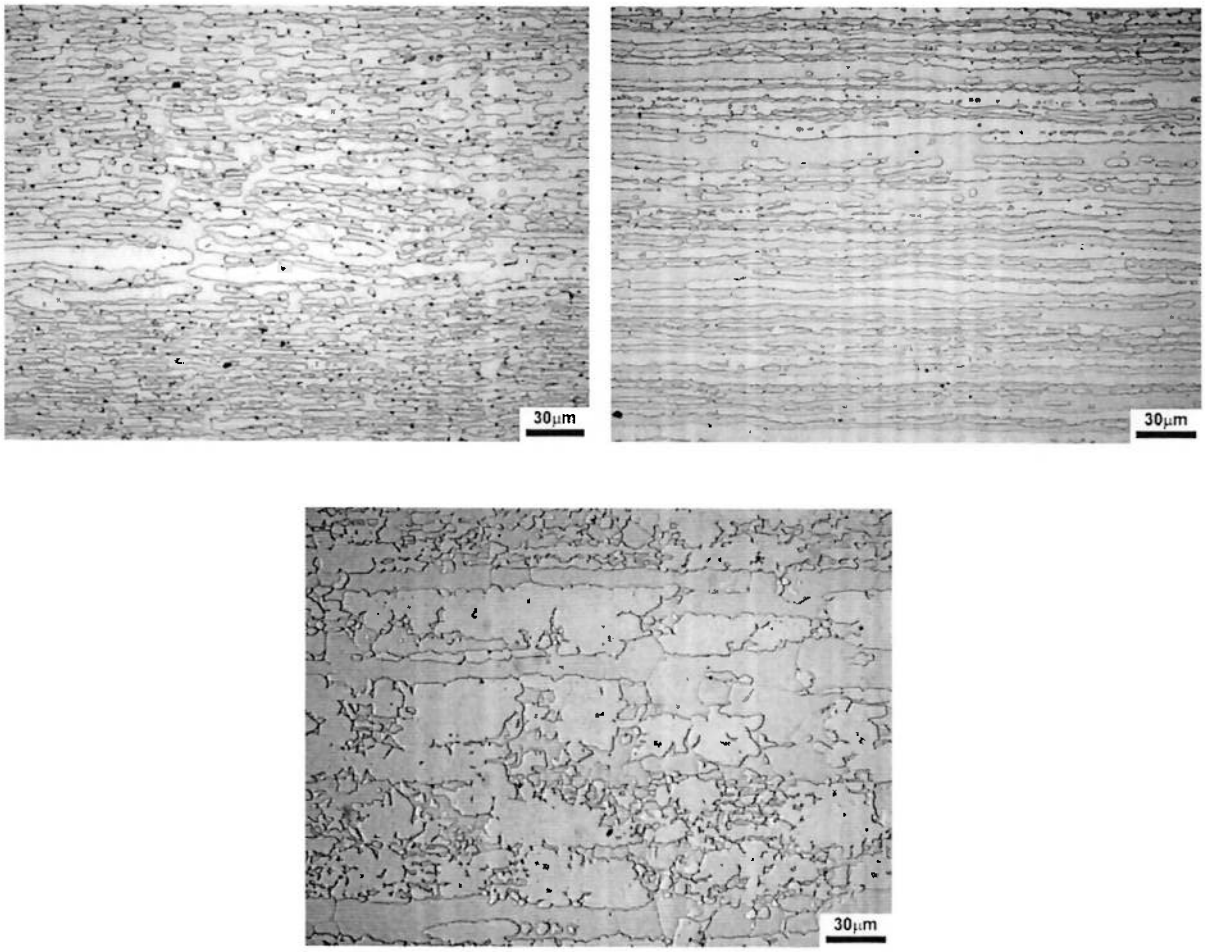

Figure 18. Transverse (up left), Longitudinal (up right) Superficial (bottom), sections for as-received rolling plate of 3mm thickness. Images taken with optical microscope, 500x magnification.

A clear lamellar structure in the longitudinal section (up right) is observed, in which austenite (bright grey) lamellae thickness varies from a few microns to 15 microns approximatvely. Concerning the transverse section, the phases are also oriented, but instead of lamellae, shorter elongated austenite grains are present inside a ferrite matrix. The surface section, is coherent with the precedent description since corresponds to the top view of the lamellas. Inside both austenite and ferrite some grain boundaries can be detected. In all the images it

can be seen that some fine austenite lamellae are broken and very fine grains of austenite are dispersed inside ferrite. In summary, this DSS micro structure could be described as flatten fibres of austenite inside a ferrite matrix. (Some black points at the grain boundaries can be present due to some inappropriate sample grinding or polishing, but they must not affect in the microstructure interpretation).

5mm thickness rolling plate

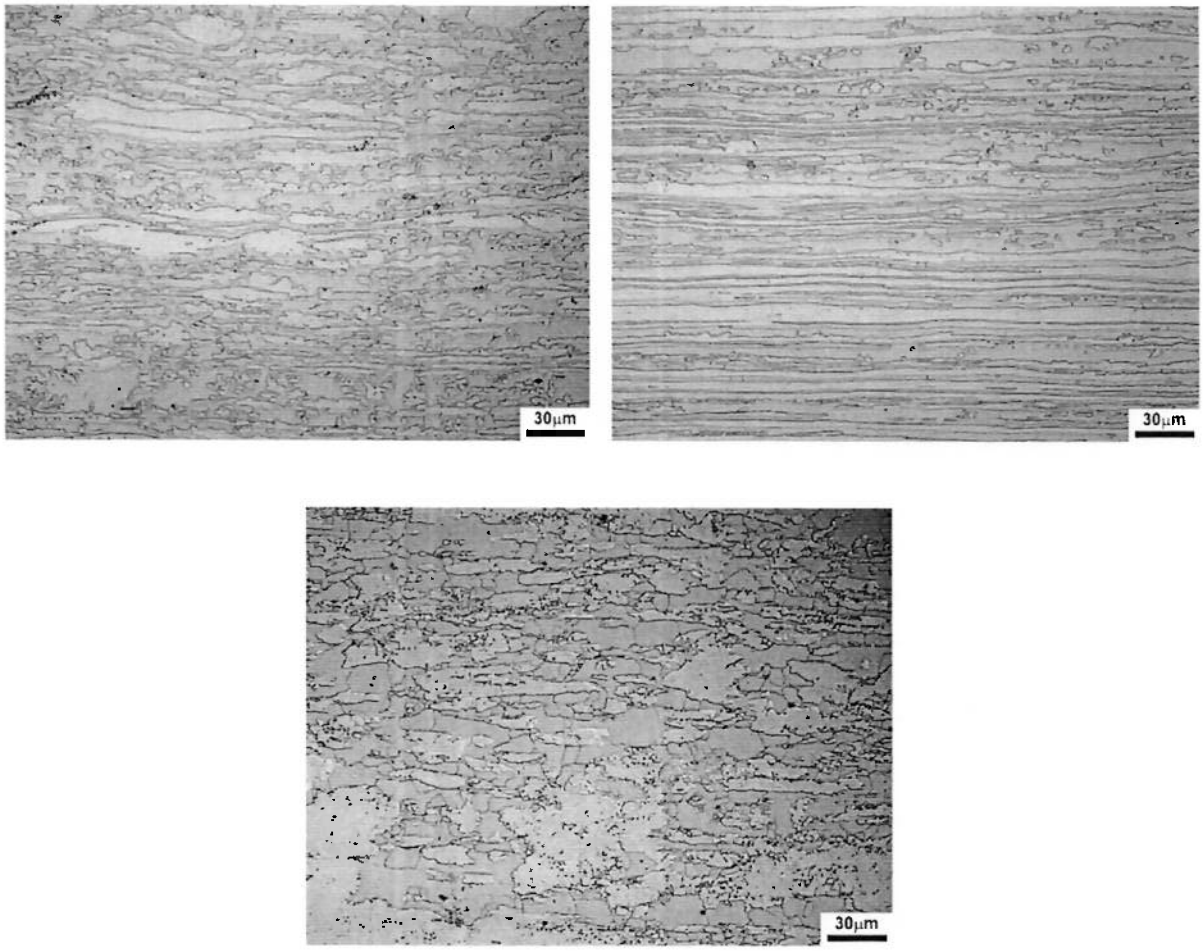

Figure 19. Transverse (up left), Longitudinal (up right) Superficial (bottom), sections for as recieved rolling plate of 5mm thickness. Images taken with optical microscope, 500x magnification.

Microstructure and lamella thickness of 5mm rolling plate sample is similar to the above described 3mm rolling plate sample. Some differences are: higher grain size variability (observed in the transverse section) and softer interphase boundary in the lamellas (observed in the longitudinal section). This last effect could be produced by the difference in thickness of the rolling plates, by some eventual different rolling process conditions or simply by a slightly different effect due to the surface attack of the samples.

6mm thickness rolling plate

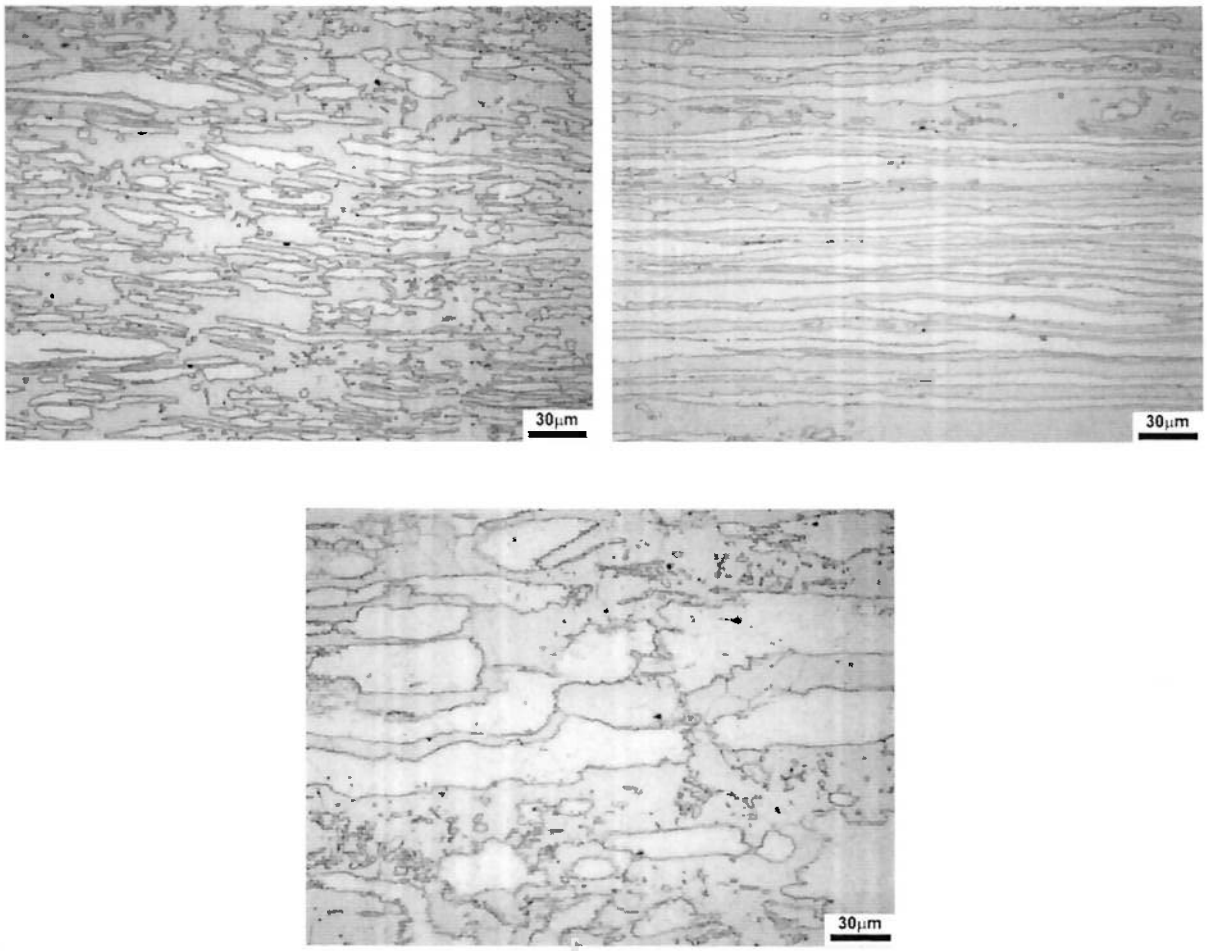

Figure 20. Transverse (up left), Longitudinal (up right) Superficial (bottom), sections for as recieved rolling plate of 6mm thickness. Images taken with optical microscope, 500x magnification.

In the 6mm rolling plate sample, preferential orientation in the longitudinal section can be observed as well. In this case, however phases are much more clear due to decrease of fine grains dispersed into the ferrite matrix (as seen in previous 6mm and 5mm cases). Lamellae thickness and grain size in general seem to be bigger than in the precedent rolling plate samples, but a quantitative analysis should be performed in order to verify this hypothesis.

10mm thickness rolling plate

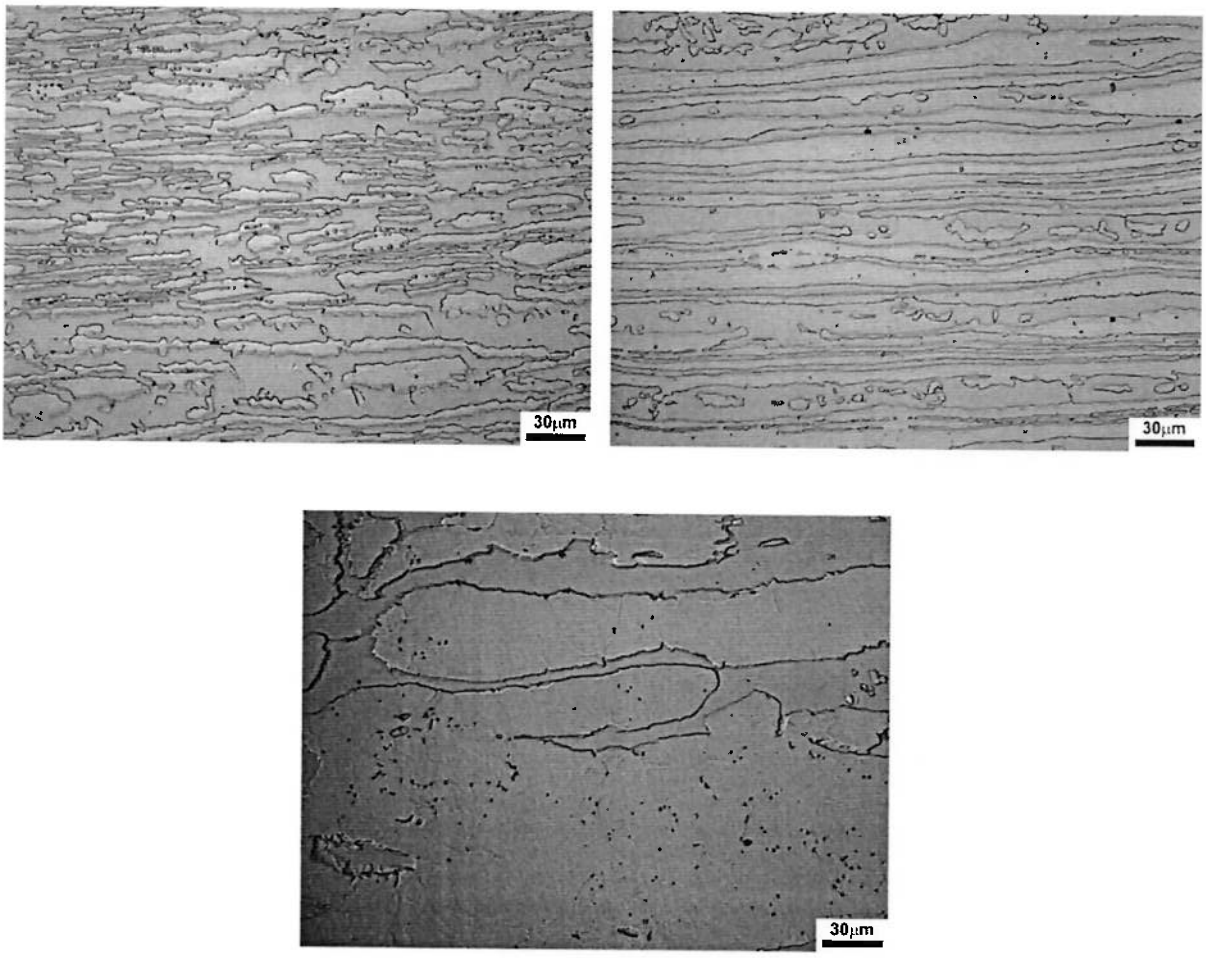

Figure 21. Transverse (up left), Longitudinal (up right) Superficial (bottom), sections for as recieved rolling plate of 10mm thickness. Images taken with optical microscope, 500x magnification.

The most relevant observation we can appreciate in the 10mm rolling plate sample is bigger grain size respect to the precedent cases. That is coherent with the idea that during rolling conformation of the plates, the more the compression applied for the rolllers on the surface of the plates, the higher the deformation inside the material and the thinner and more fractured lamellae is expected.

After having analysed all the images of all samples we could conclude that DSS rolling plates could be considered as a composite material with ferrite matrix and flattened fibres (or lamellas) of austenite as a reinforcement. The lamellas are much more elongated in the longitudinal direction than in the transverse. That anisotropy is expected to play a role in the mechanical behaviour of these duplex materials.

Cylindrical Sample

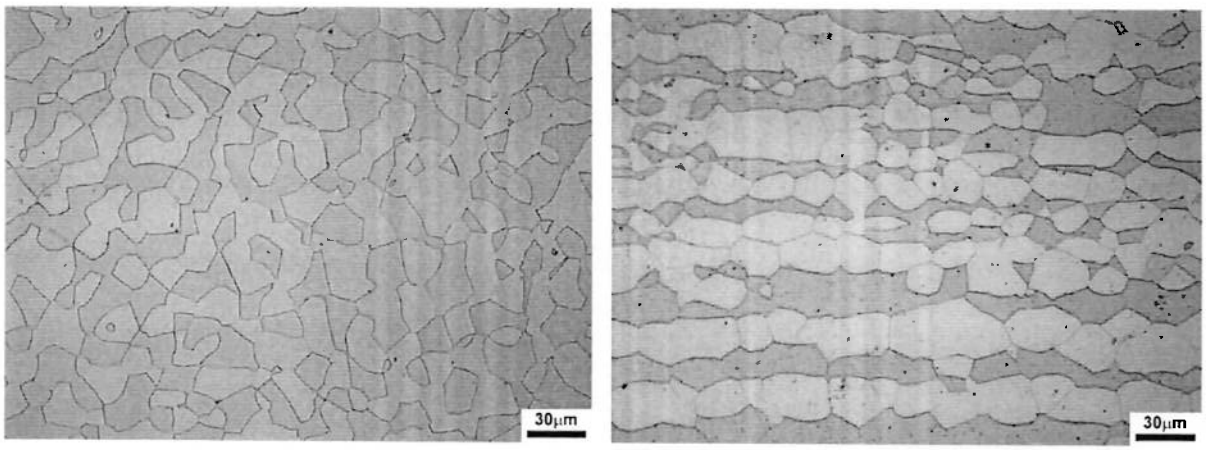

Figure 22. Transverse (up left), Longitudinal (up right) Superficial (bottom), sections for cylindrical specimen. Images taken with optical microscope, 500x magnification.

Cylindrical sample presents axisymmetric microstructure, therefore just two sections are needed to characterize the sample. In the normal (or superficial) section the equiaxial character of phases is well observed. In the longitudinal section, clear preferred orientation can be observed and the lamellae thickness appears to be much higher than in the rolling plate cases.

In the Figures 23 and 24, 3D photomontages of all the samples are presented in order to better understand its microscopic disposition:

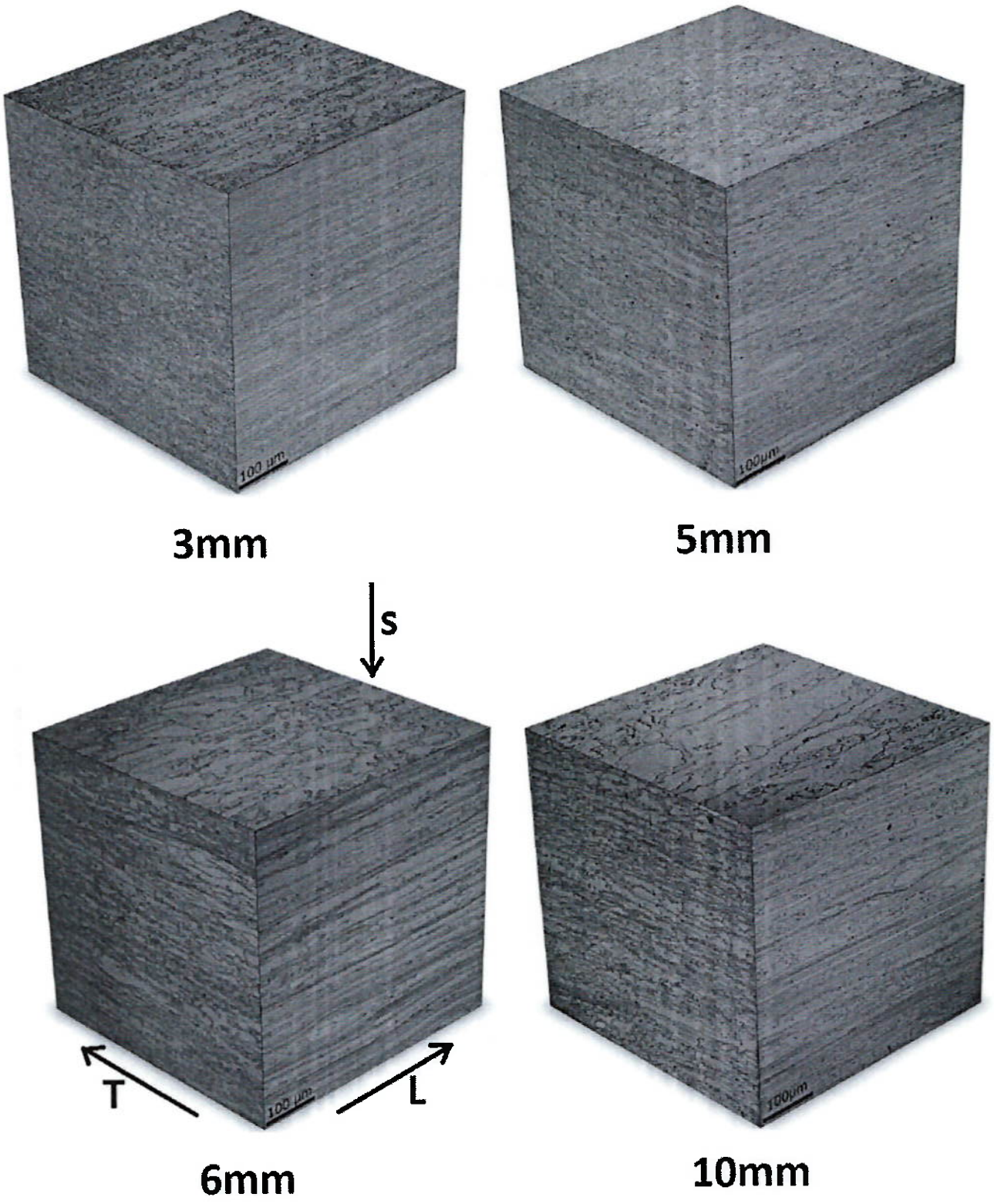

Figure 23. Photomontage with microstructures in the Longitudinal (L), Transverse (T) and Superficial (S) directions for the different rolling plate specimens. Rolling plate thickness specified under each cube. Magnification 200x.

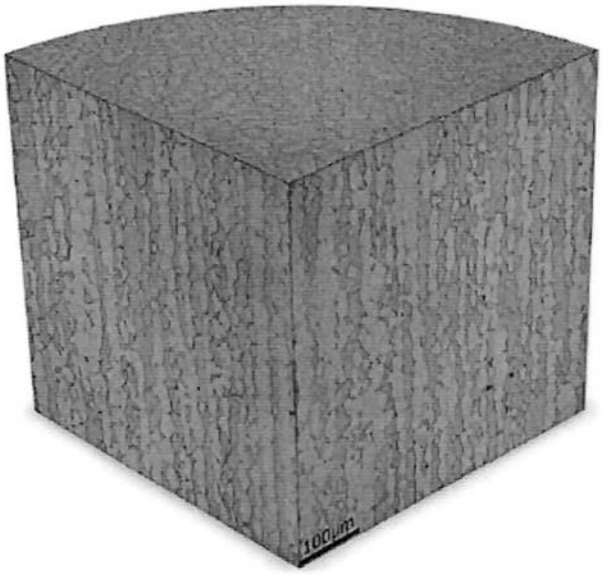

Figure 24. Photomontage with microstructures in the Longitudinal (L), Transverse (T) sections for the cylindrical specimen. Magnification 200x.

5.3. Tensile tests

After performing the tensile tests to 10mm and 6mm thickness specimens, the following curves have been obtained:

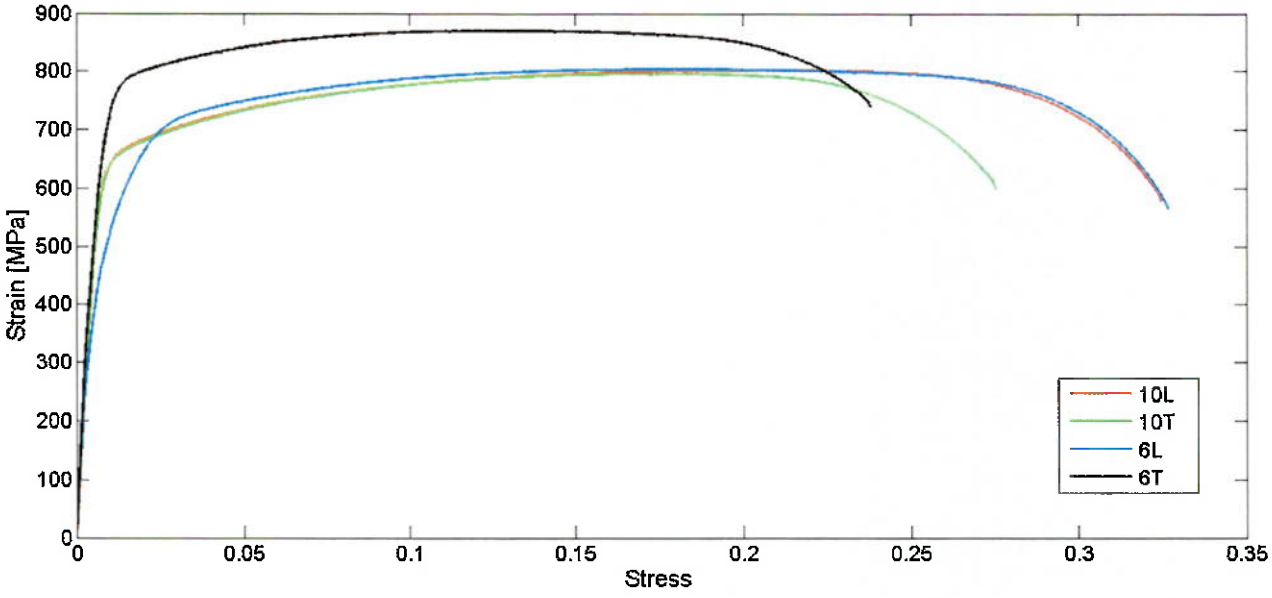

Figure 25. Engineering Stress vs. Strain curves derived from the tensile tests. 10mm Longitudinal in red, 10mm Transverse in green, 6mm Longitudinal in blue, 6mm Transverse in black.

The parameters derived from the curves above are presented in the following Table 9:

Table 9. Mechanical properties dervided from the tenisle test curves. Tests performed to 10mm and 6mm thickness rolling plates, both cut in the longitudinal and the transverse direction.

	E [GPa]	Ultimate Tensile Strength [MPa]	Uniform Elong[%]	Breaking Strength [MPa]	Total Elong[%]	Yield Strenth 0,002 [MPa]
10mmL	98,33	802,91	17,91	578,29	31,86	615,11
10mmT	103,02	796,48	16,9	598,99	26,92	597,28
6mmL	84,67	804,42	17,03	566,11	31,99	461,98
6mmT	114,47	871,13	12,42	740,28	23,14	638,33

Concerning the Young Modulus, the two transversal cut specimens present higher values.

The uniform elongation value (plastic deformation occured before neck formation) is higher for 10mmL and 6mmL, meaning that the longitudinal specimens allow more homogeneous

deformation inside its microstructure before deform heterogeneously forming the neck. The longitudinal disposition respect to the load direction of the lamellas is more susceptible to be deformed.

Concerning the Ultimate Tensile Strength the 6mm thickness transverse specimen has higher value (871 MPa), what is a significant difference in respect to the other three, that have approximately the same values (around 800 MPa). This increase is expected to be produced by the combination of the grain size effect (grain size in 6mm samples is slightly smaller than in 10mm samples) plus the transverse orientation effect of the lamellas.

All these results suggest deforming duplex stainless steels with the lamellas perpendicular respect to the applied force is more difficult. In other words, phases have more difficulties to flow during plastic deformation when lamellas are transverse to the applied stress.

Considering that duplex stainless steel is a two-phase ductile material that experiments certain "flow" of the phases before fracture, and that deformation is easier to transfer inside the same phase than from one phase to another, a possible explanation for the results obtained in the tensile tests could be the following hypothesis:
For longitudinal specimens, the material inside each phase can flow (in other words, propagate its dislocations) inside its own lamellas, delimited by the α/γ interphases, which would act like elongated containers or "pipelines" for each phase.
Therefore flowing in the longitudinal direction for a phase will be easier because less interphases, or in other words "obstacles", will be encountered by dislocations along its advancement. And on the other hand flowing in the transverse direction would be more difficult due to higher interaction of the material inside a phase with interphase boundaries.

Accordingly, long continuous lamellas (in the direction of the load) would promote higher deformation than non-continuous ones.
It is well known that grain size effect plays a role in the mechanical behaviour of materials. In DSS case, smaller grain size could increase the effect of "obstacles" encountered by the flowing material, increasing its mechanical strength and reducing total elongation.

The sum of the transverse orientation of lamellas respect to the applied load added to the fact that 6mm thickness rolling plate, in principle, has small lamellae than 10mm thickness rolling plate would explain why the 6mmT specimen has showed a clear improvement in strength and less ductile behaviour than the rest.

In the following Table 10. the results derived of the tensile test of the cylindrical specimen are presented. For this sample it was not possible to record the stress vs strain curve, consequently, only some parameters are in the Table.

Table 10. Results of tensile test of cylindrical specimen.

Initial Diameter [mm]	Initial cross-section Area [mm2]	Ultimate Tensile Strength [MPa]	Total Elongation
8,2	52,81	840	37%

The Ultimate Tensile Strength for this specimen, with a value of 840 MPa, is coherent with the results obtained for the rolling plate samples.

Concerning the plastic elongation at fracture, it presents the highest value among all the tested specimens in this study. That fact could be consistent with the hypotesis stated in the lines above, in which it has been explained that longitudinal oriented specimens, with long and big size lamellas (all these factors were present in this cylindrical specimen) would present higher deformation values before fracture.

5.4. Metallography of after-tested specimens

5.4.1. Cylindrical Specimen

After performing a tensile test to the cylindrical super duplex specimen, a metallographic analysis allows to investigate different phenomena derived from the deformed microstructure.

Figure 26. Mounted cylindrical after-tested specimen. Longitudinal section. Neck with fracture can be observed in the right side. Load direction: horizontal.

Globally for the cylindrical specimen, and as it can be clearly observed in APPENDIX A, the evolution of the microstructure from homogeneous deformed region to fracture region is the following:

- Progressive change in lamella orientation as long as they approach to the neck zone.
- Quasi disoriented lamellas jest before the neck region.
- Highly oriented and deformed lamellas in the nech region.
- Just before fracture, disoriented lamellas again.

Some of the effects observed in cylindrical specimen after fracture are further commented in the following paragraphs:

5.4.1.1. Serrated ferrite/austenite interphase boundaries

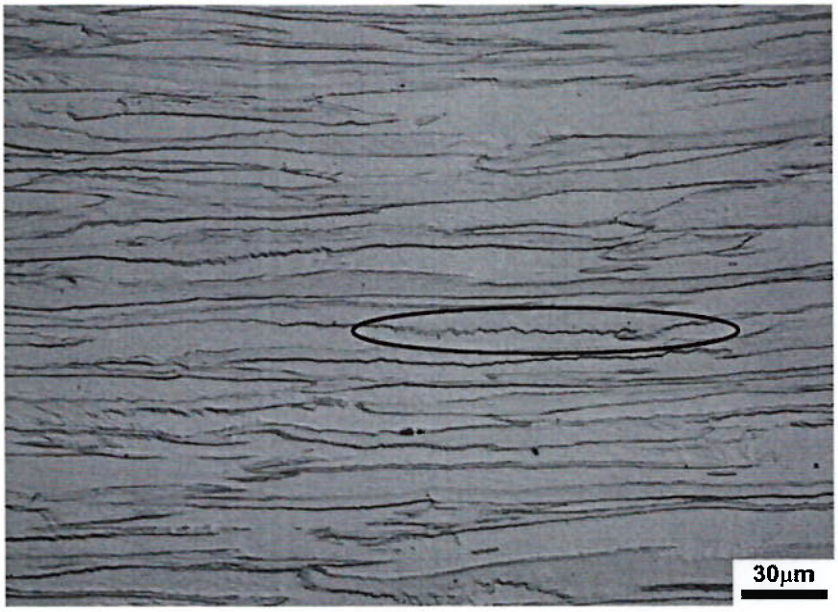

Figure 27. Serrated Interphase Boundaries in the interphase between ferrite and austenite. Load direction: horizontal.

Due to the different deformation mechanism of ferrite and austenite, some stress concentrations will be accumulated their interphases. This incompatibility in the deformation would explain the serrated grain boundaries shown in the image above.

5.4.1.2. Deformation bands inside austenite and ferrite

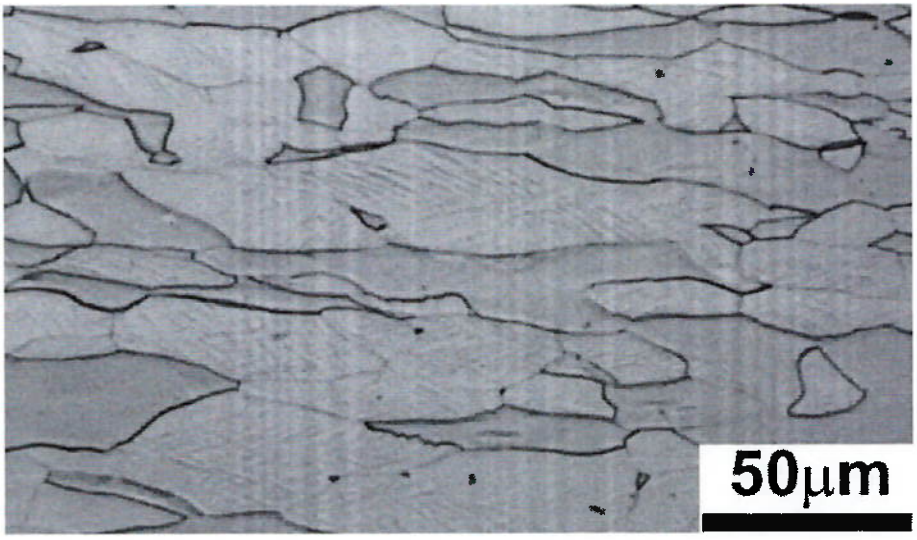

Figure 28. Deformation bands in austenite phase. Parlallel and crossed slip bands oriented 45º approx to the load direction. Load direction: horizontal.

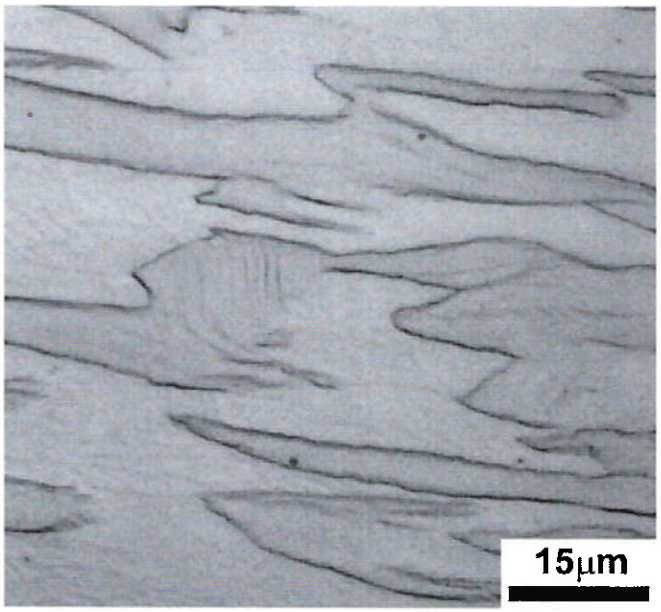

Figure 29. Deformation bands in ferrite phase. Parallel curved slip bands. Load direction: horizontal.

In the Figures 28 and 29 it can be observed the clear difference in deformation of austenite and ferrite respectively. The first one deform in straight slip bands that seem to flow at 45º approximatively with respect to the load direction, due to shear stresses. The second, can deform with curved slip bands that can even be perpendicular to the direction of the applied load.

5.4.1.3. Different regions of plastic deformation

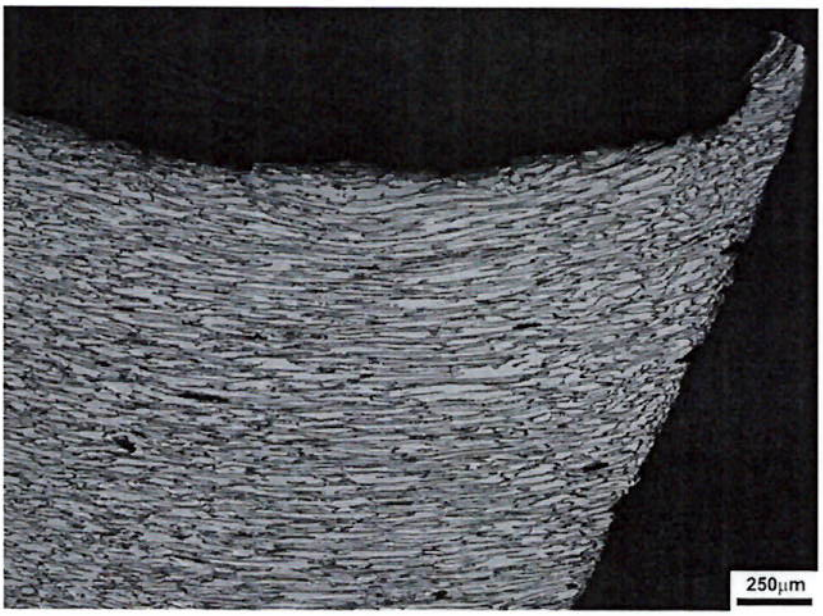

Figure 30. 3 regions of deformed lamellas close to the fracture (right side).Load direction: horizontal.

A possible explanation to these different regions of different morphology, following the thesis purposed in 5.2 could be the following:
When some lamellas close to neck region are strongly oriented due to high deformation (as it can be seen in the central part of Figure 30), they are as well strongly hardened by cold deformation. These highly deformed lamellas do not allow more material flow inside or between them, generating some kind of microscopic "wall" for dislocations close to the neck region.

The lamellas in other regions that have not been as much cold worked as the first ones, and could still deform (left part of Figure 31), lose its orientation when encounter the barrier of high cold worked lamellas. This sudden change of orientation in some lamellas could generate stress accumulation in the interphases between ferrite and austenite leading to micro voids formation.

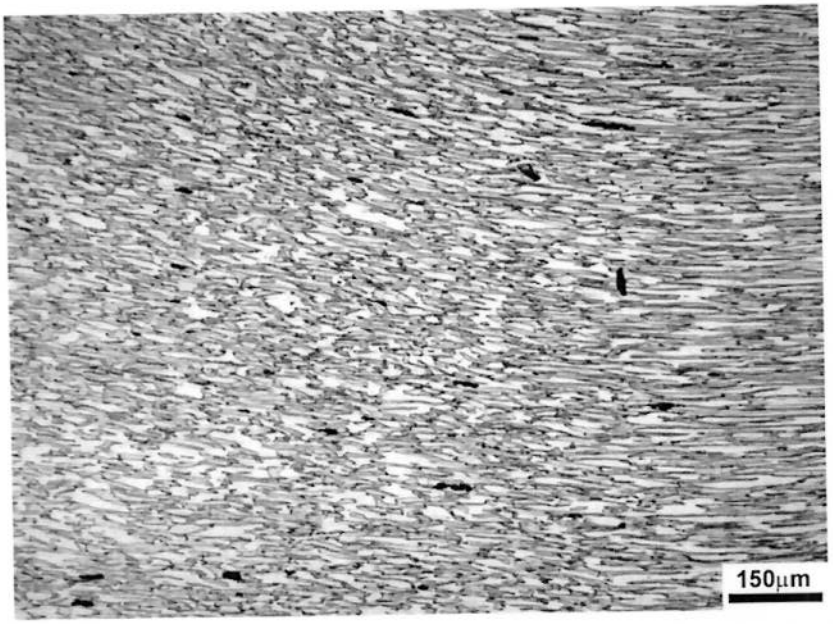

Figure 31. Misoriented grains experiment a drastic elongation in the neck region. Fracture in right side. Load direction: horizontal.

5.4.1.4. Micro voids formed in the neck region

It has been verified, with the photomontage in Figure 32, that microvoids are formed in different parts of the material before fracture, as stated in the literature. These micro voids are more concentrate and have bigger size in the neck region close to the fracture. The rupture of the material it is expected to happen along one propagated facture starting from one of these microvoids.

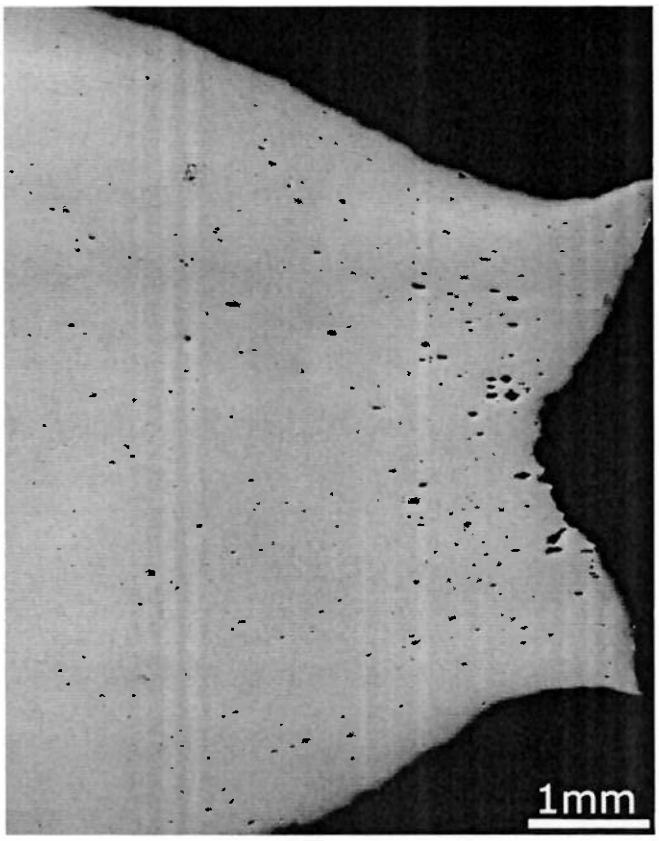

Figure 32. Increasing population of micro voids in the neck region of fractured cylindrical specimen.

5.4.1.5. Micro voids formed in the ferrite/austenite interphase

As it can be seen in the following images, micro voids formed during high plastic deformation near the fracture zone are always in contact (or almost in contact) with the interphase between ferrite and austenite. The voids appearing inside a phase are expected to have nucleated near the interphases as well. This phenomena is coherent, for example, with the thesis stated by [Makinde, 1986]: for a state of uniaxial stress in a two-phase material, the difference between the anisotropies of the phases present gives arise to a biaxial stress state in each phase.

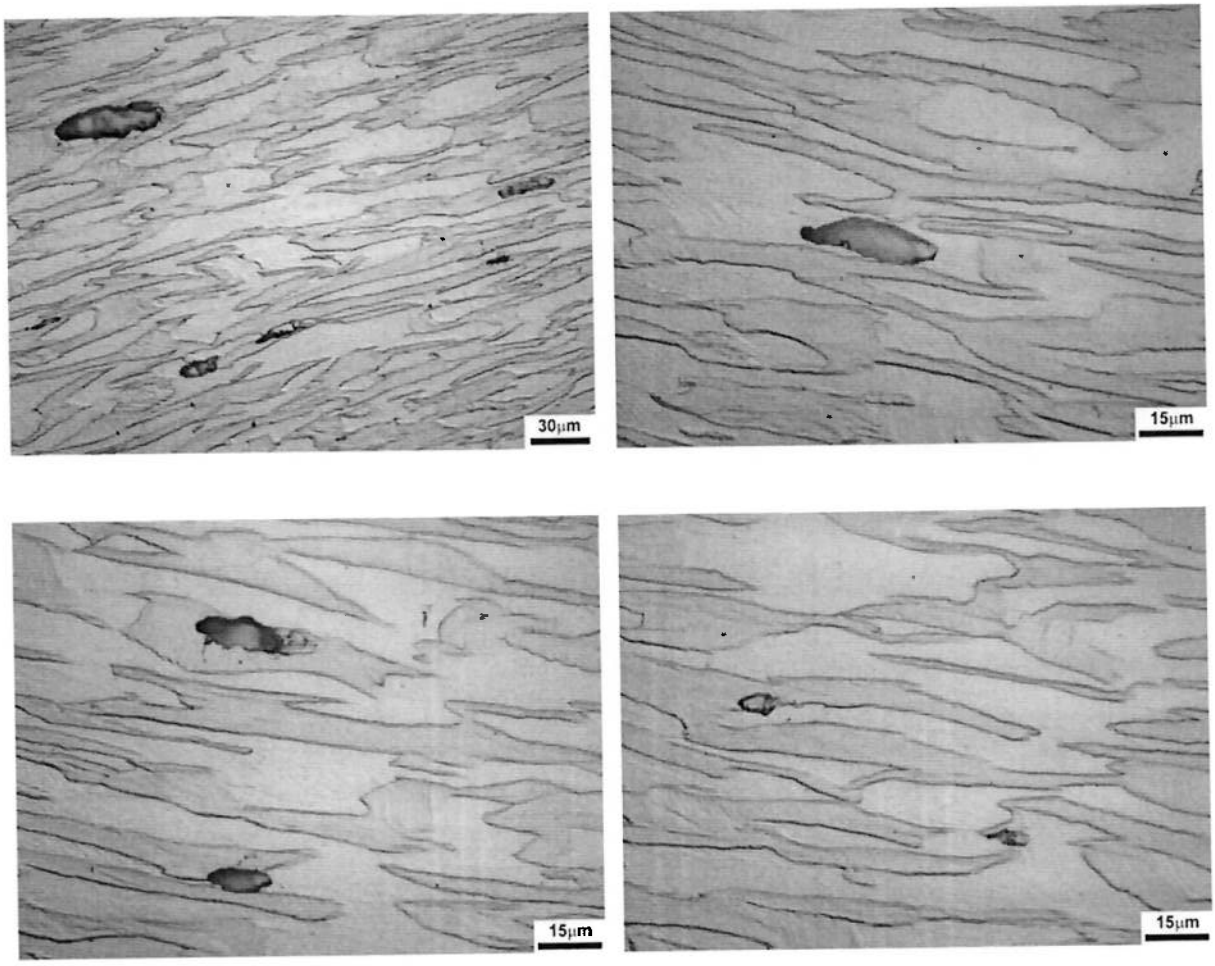

Figure 33. Micro voids close to ferrite-austenite interphases.

5.4.1.6. Macroscopic shear band

A clear shear band can be observed in the microstructure near the fracture region (right part of the Figure 34). The angle of the shear band is 45° approximately respect to the load direction (horizontal). This shear band may be formed during necking of the sample before fracture.

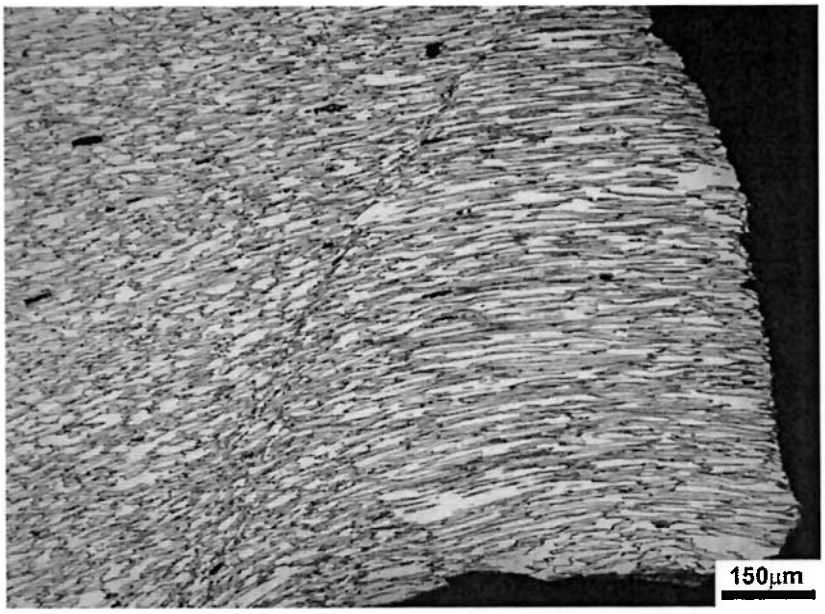

Figure 34. Shear band observed at 100x.

A shear band and two different deformation regions clearly are observed in Figure 34. The shear band seems to be a barrier between high deformed an oriented lamellae, close to the fracture (right part of the image) and less deformed and more equiaxial grains. The material is expected to fail through sliding on shear bands like this one. What could have happened in this sample, is that fracture has taken place in another more developed shear band, leaving this one quite well developed and visible almost to the naked eye.

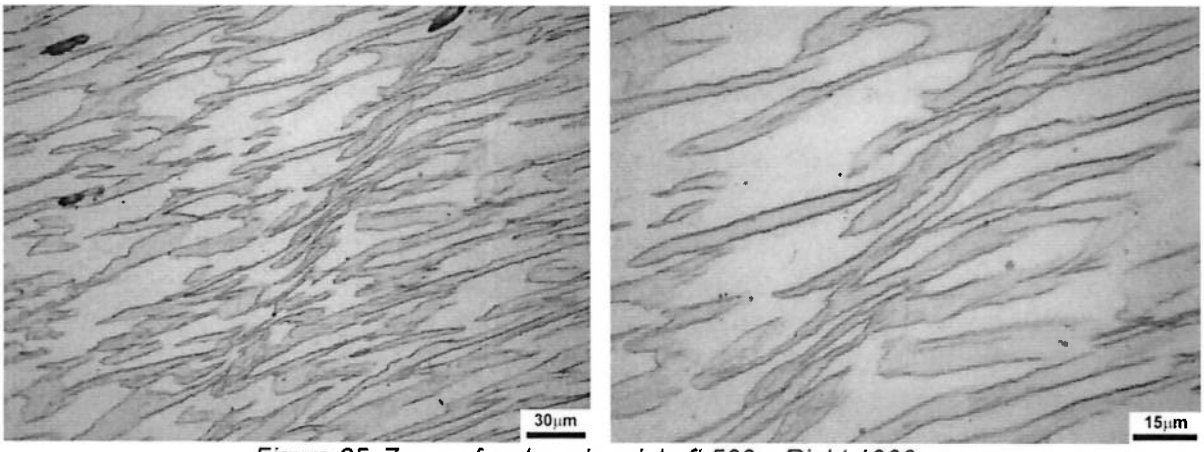

Figure 35. Zoom of a shear band. Left 500x. Right 1000x..

Note that austenite zones (bright grey) are much wider than ferite ones (darker gray), indicating that ferrite has a higher "flowing" effect during deformation and in consequence it should be more ductile.

5.4.2. Rolling plate specimens

The region observed in the figure 36, which is close to the fracture, presents a microstructure similar to the transverse section of the as-received rolling plates analysed above. However, the microstructure presents an undulation distortion in the load direction. That could be induced for the high quantity of interphases that the transversal lamellae encounter when they deform in the horizontal direction due to the applied load.

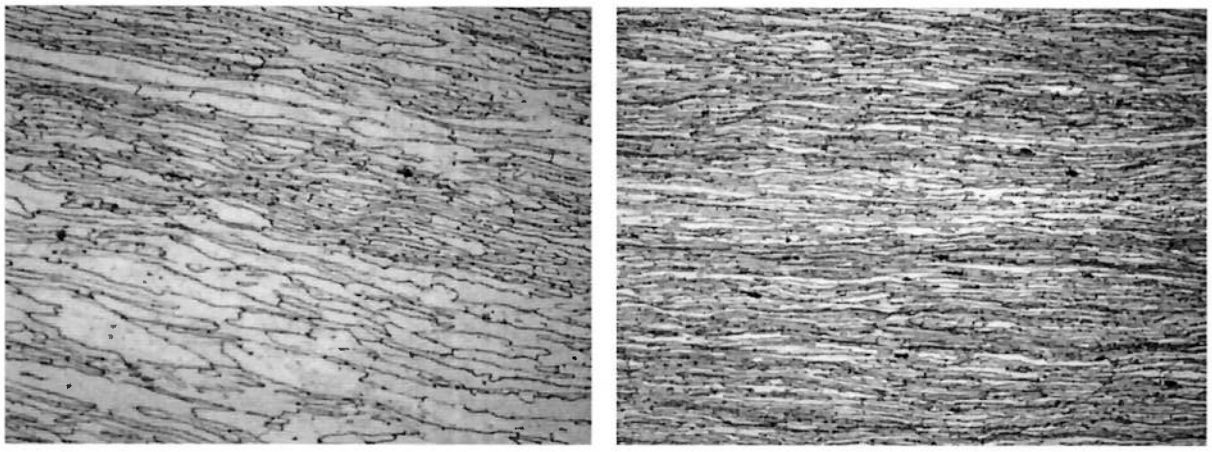

Figure 36. Undulation phenomena observed in 10TEsp - 10mm rolling plate observed in a surface parallel to thickness. Magnification 500x. Load Direction: Horizontal.

Figure 37. corresponds to a top view of a trensverse cut specimen after deformation in a tensile test. At right image (deformed region) it can be observed that lamellae are much thinner thar the ones on the left image (non deformed) and they present a pronounced distortion. This effect is produced close to the fracture zone due to high heterogeneous plastic deformation. Successive parallel lamellae are accumulating perpendicularly to the load direction. The interphases preserve approximatively the initial number of lamellae, but they are all condensed and distorted.

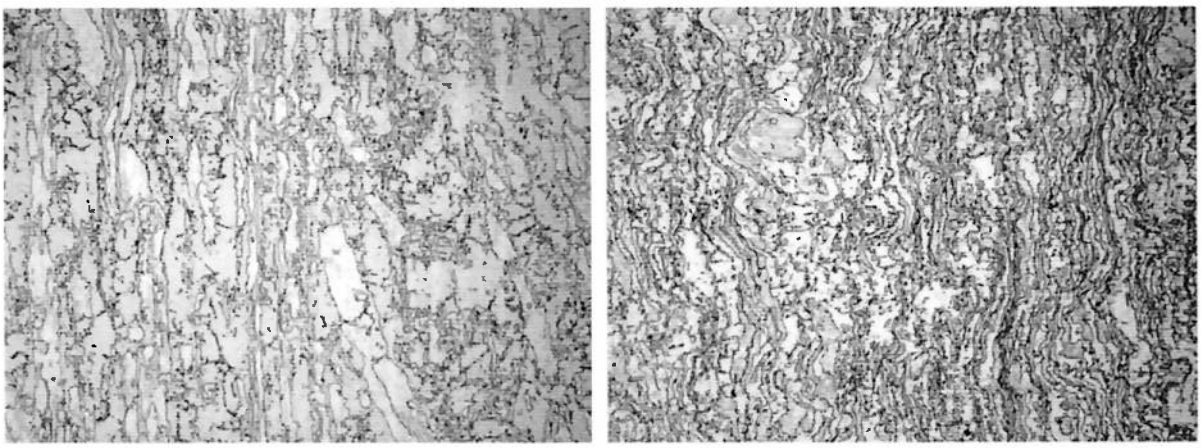

Figure 37. Distortion of the lamellae observed in 6TLarg: 6mm Transverse cuted specimen observed in a surface perpendicular to thickness. Left image (non-deformed region) 100x magnification. Right image (deformed region close to fracture), 100x magnification. Load Direction: Horizontal.

In Figure 38. It can be observed a surface parallel to thickness of a 6mm longitudinal cut specimen, after deformation in a tensile test. It is clear that lamellae "fit" without serrated boundary distortion inside the specimen, along the uniform deformed region and even in the fracture region. From this pictures it can be stated that lamellas "flow" better when they are oriented in the same orientation as the applied force (they do not present high distortion or undulation in the interphases, they are not broken or change orientation suddenly).

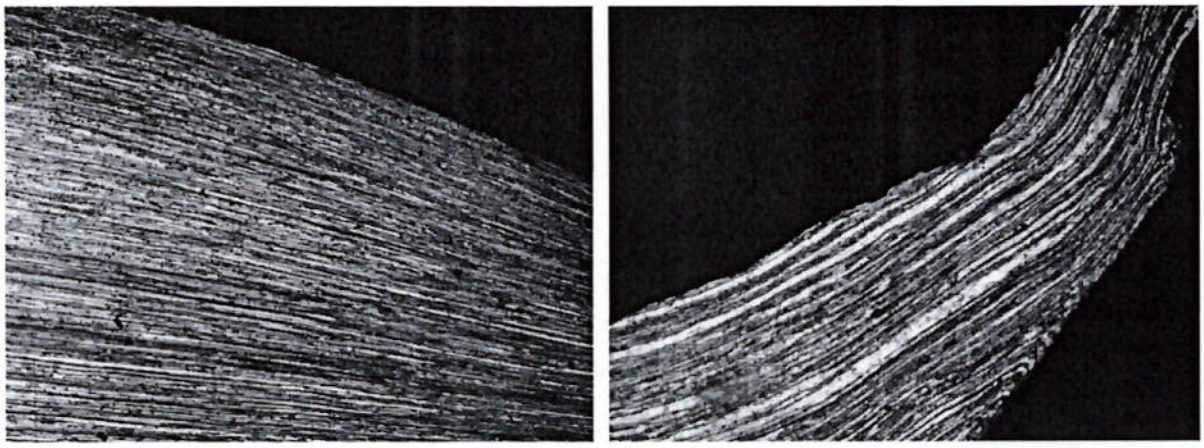

Figure 38. Lamellae fit in the neck deformed region observed in 6LEsp - 6mm rolling plate observed in a surface parallel to thickness. Left image (start of neck region) 50x magnification. Right image (facture zone)500x magnification. Load Direction: Horizontal.

In summary, it could be noted as hypothesis that lamellas are more likely to allow deformation in the material when they are parallel oriented to the applied load, rather than they are transverse oriented to the force.
The main difference between the rolling plate samples with the cylindrical specimen is the initial thickness of the lamellae. For rolling plate samples, the lamellas were much thinner.

It has been observed that wide lamellae deformation might be more complex than deformation in thin ones, since in the cylindrical specimen different regimes of plastic deformation have been observed (progressive change in lamella orientation, followed by completely disoriented lamellas, then highly oriented and deformed lamellas, and finally, just before fracture disoriented lamellas again).
In consequence, we can state also as hypothesis that lamellae thickness plays an important role in plastic deformation.

5.5. Hardness

Results of Hardness measured in ferrite and austenite for a DSS and a super DSS are presented in the following Table 11.

Table 11. Vickers micro hardness results for austenite and ferrite phases in duplex UNS S32304 and super duplex UNS S32750

Duplex Grade	**UNS S32304**		**UNS S32750**	
Phase	**ferrite**	**austenite**	**ferrite**	**austenite**
$HV_{0,01}$	236	332	324	316
	263	332	316	309
	269	316	309	324
	275	358	324	316
	269	340	316	309
	257	349	316	349
	269	340	324	324
	257	332	309	309
	269	316	316	309
	253	358	316	340
Average	**261,70**	**337,30**	**317,00**	**320,50**
Std. Deviation	**11,41**	**14,91**	**5,58**	**14,09**
Significative difference 95% confidence	YES		NO	

As the indentation generated by the tip indenter produces a triaxial strain on the surface of the specimen, the measures are not strongly affected by orientation of the phases present in the microstructure; in other words, anisotropy should not affect the hardness test results.

Some influence of the grain boundaries could produce some bias in the measures of austenite in UNS S32304. That is because it has not been possible to perform the indentations far from the grains, due to the fine thickness of austenite lamellas. Therefore, the hardness measures for austenite in UNS S32304 may include some influence from ferrite hardness.

Regarding the results from Table 11. the austenite in UNS S32304 DSS is harder than ferrite, more specific a 28,89% harder. That seems coherent with the fact that ferrite, that is organized as a BCC primitive cubic system, has more slip systems (48) than austenite (12). The more slip systems the more the probability to glide following one slip direction when the microstructure is under stress.

On the other hand, in the super DSS ferrite and austenite average hardness do not present significative difference. That similar hardness could be induced by the higher alloy element content in the UNS S32750. As it can be seen in the tables 4 and 5 of point *4.1 As-received material,* ferrite former elements are strongly increased in super DSS in comparisoon to DSS, for example Cr (12%+ approx.) and specially Mo (1200%+ approx.). The austenite former elements have to be considered as well, with an increase of Ni (90%+ approx.) and N (170%+ approx.). Despite this, the extremely high increase in Molybdenum amount could be the main explanation to the similar hardness of ferrite and austenite.

5.6. Fracture region analysis

In Figure 39. the fracture parts of rolling plate samples have been photographed at the same magnification in order to compare them.

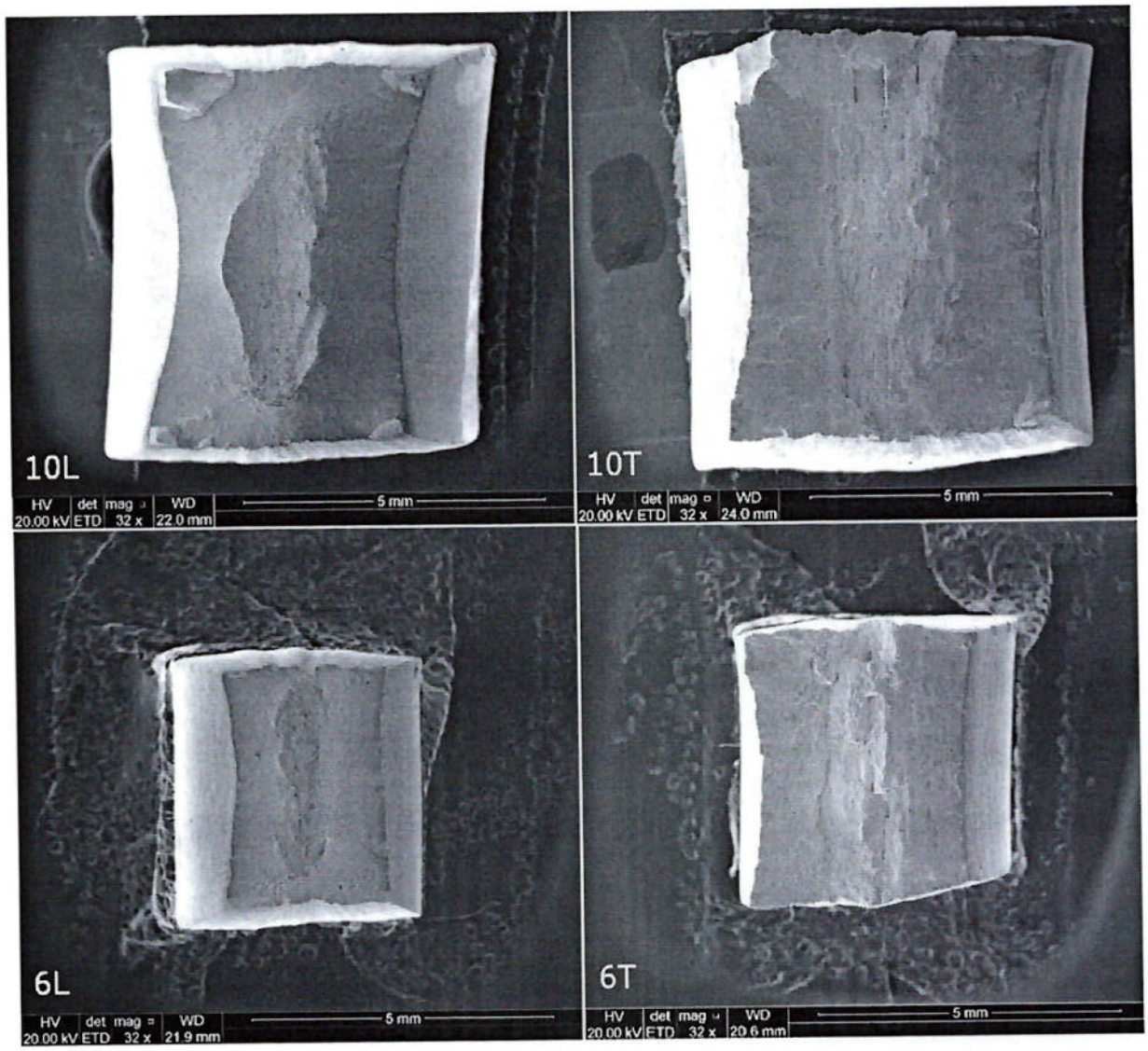

Figure 39. Top view of the fractured rolling plate specimens after tensile test. 32x magnification. Horizontal dimension: Thickness; Vertical dimension: Width. Review the Figure 15 to better understand the lamellae disposition.

In the following Table 12, the cross section of fracture, the minimum width and the minimum thickness of the specimens are presented:

Table 12. Area, minimum width and minimum thickness measured to the fractured UNS S32304 samples. In pixels and in mm.

	Area [pixels]	Min. width [pixels]	Min. thickness [pixels]	Area [mm²]	Min. width [mm]	Min. thickness [mm]
10L	1184984	1380	782	24,89	6,32	3,58
10T	1581880	1384	1052	33,22	6,34	4,82
6L	479502	852	530	10,07	3,90	2,43
6T	750292	920	720	15,76	4,22	3,30

Table 13. Area reduction, thickness reduction, width reduction and plastic strain ratio for the different rolling plate samples.

	Area Reduction [%]	Max Thickness Reduction [%]	Max Width reduction [%]	Plastic strain ratio (Width/ Thickness)
10L	-74,32	-64,86	-33,43	1,75
10T	-64,48	-51,46	-32,64	1,31
6L	-72,77	-60,93	-34,38	1,61
6T	-58,31	-47,62	-29,73	1,28

Apparently tensile test specimens cut in the rolling direction (10L and 6L) present a higher area reduction during neck formation, and that is due especially to a higher thickness reduction.

We could conclude after analysis of the results of Table 13 that longitudinal oriented specimens (with respect to the load), allow more thickness deformation, due to an easier reduction in lamellas thickness during plastic strain. On the other hand thickness reduction for transverse oriented specimens (with respect to the load), is expected to be much difficult. The higher reduction in thickness in Longitudinal specimens (10L and 6L) explains as well their higher Area reduction and higher plastic strain ratio.

Concerning the cylindrical specimen, the fracture appearance is presented in the following Figure 40.

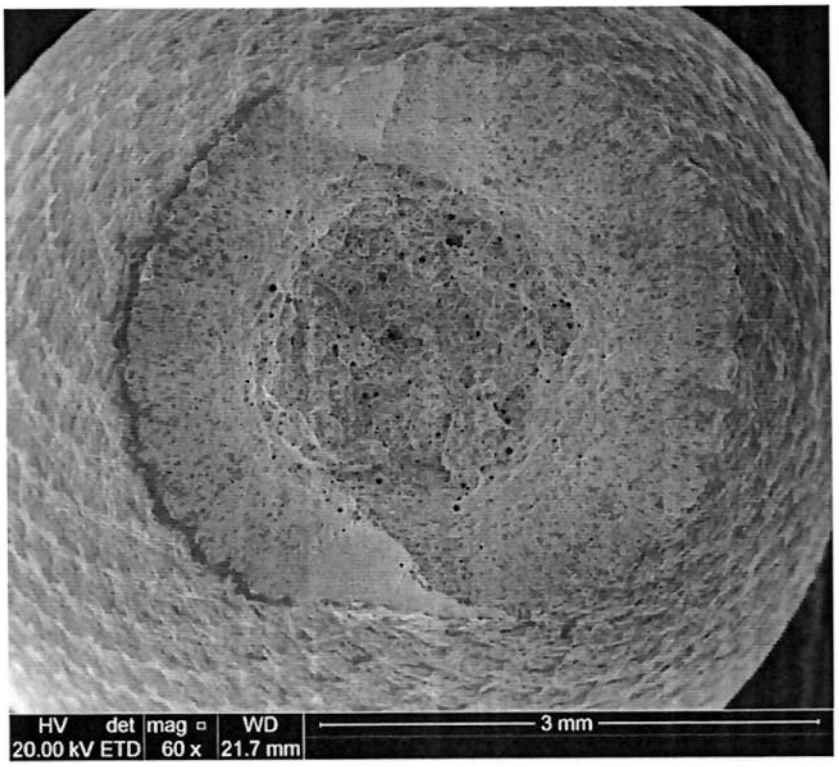

Figure 40. Top view from the fractured cylindrical specimen. SEM image. Magnification 60x.

In this case no anisotropy appears in the neck fractured region, since the final cross section of the specimen is circular as the before-tested one.

Two main regions can be observed, the exterior ring seems to be fractured by shear stress. At the top and the bottom of the ring two clear shear bands can be observed, giving the impression, even that the fracture has been produced by torsion. In the circular central part, higher concentration of micro voids can be observed, and the rupture seems to have occurred in a more fragile way.

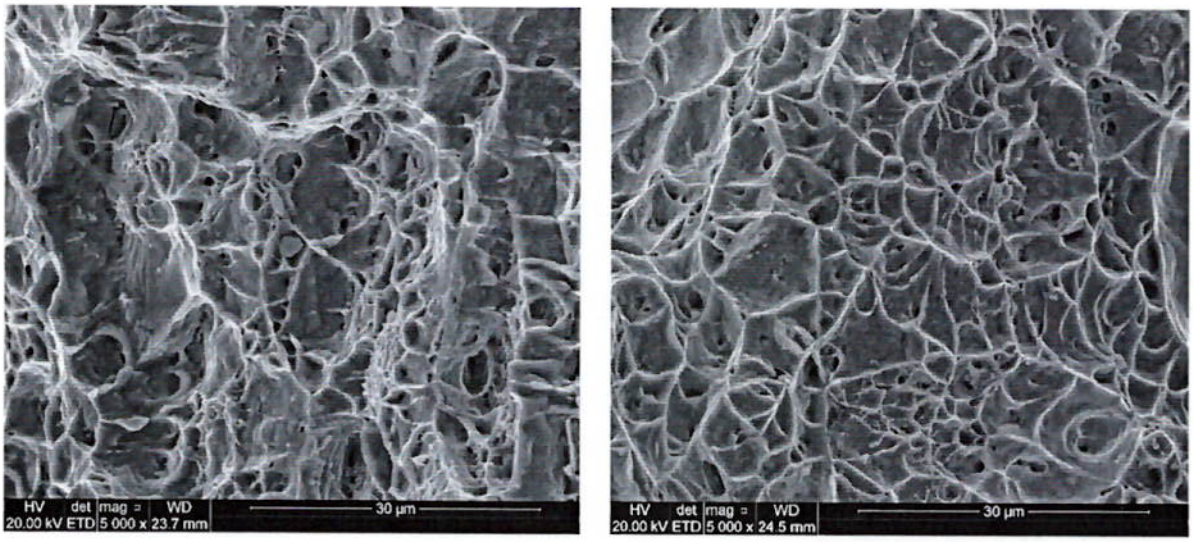

Figure 41. Fracture of 10T specimen. Left image corresponds central part of fracture, 5000x ; Right image corresponds to a side of the fracture, 5000x.

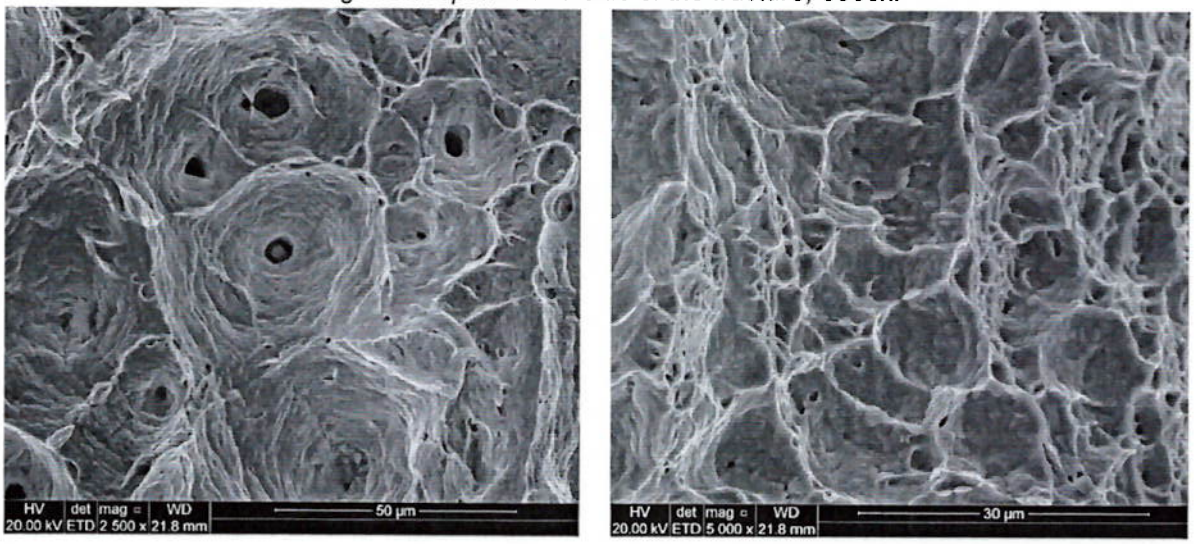

Figure 42. Fracture of Cylindrical specimen. Left image corresponds central part of fracture, 2500x ; Right image corresponds to a side of the fracture, 5000x.

The main difference between the rolling plate samples and the cylindric one is that the first ones have smaller micro voids in the central part of fracture (left images), and they also present a more sharpened dimpled pattern than the cylindrical one (that has "softer" circular dimpled boundaries). Is fact is expected to be due to the 3 direction anisotropy of the rolling sheet samples versus the axisymmetric character of the cylindrical specimen.

6. Suggestions to future works

Interrupted tensile tests plus metallography analysis could be performed to appreciate better the plastic deformation behaviour of austenite and ferrite in the neck region before fracture.

Calculate the plastic strain ratio (anisotropic deformation in the neck) through tensile tests with specimens cut at different angles respect to the rolling direction (In the current work, specimens were cut just longitudinal 0° and transverse 90° respect to the rolling direction).

Quantify the anisotropy for the different samples.

Factorial analysis to study more quantitatively mechanical behaviour in function of: specimen orientation with respect to the rolling direction, rolling plate thickness and/or lamellas width.

Characterize the DSS rigidity matrix parameters. Try to characterize duplex stainless steels as a composite material.

Measure the distance of neck formation in function of lamella thickness and orientation of the deformed lamellas respect to the tensile test axis.

7. Conclusion

According to the literature it can be stated that some factors influencing the mechanical behaviour of duplex stainless steels are expected to be:

- Austenite/ferrite volume ratio.
- Lamellae morphology (thickness, width) and size.
- Lamellae respective orientation to the direction of the applied load.
- Hardness of both austenite and ferrite and particular deformation mechanisms of each phase.

Different phenomena occurred during plastic behaviour and fracture of DSS have been qualitatively analysed in this work. Among the most significant behaviours observed in after-tested UNS S32750, the following ones can be lighted:

- Serrated interphase boundary α/γ due to biaxial stress state of both phases.
- Different regions of heterogeneous plastic defomation.
- Microvoids formed at α/γ interphase boundaries.
- Fracture throug macroscopic shear bands

Cylindircal extruded samples present axisymetry, in consequence just two different sections need to be analysed (longitudinal and transverse ones). For that reason, after tensile tests, cylindrical specimens do not present anisotropic deformation in the neck, resulting in a circular cross-section at the fracture zone, as expected.

Rolling plate samples, on the other hand, present anisotropy in 3 directions (having different longitudinal, transverse and normal sections). This fact produces an anisotropic deformation during neck formation after tensile tests, resulting in a final deformed-shape rectangle cross-section from an initial square cross-section.

Higher elongation values after tensile tests and higher thickness reduction are expected to occur when lamellas are parallel oriented respect to the load direction.

Transverse cut specimens respect to the load direction and fine grain specimens are expected to be more strength and less ductile than longitudinal cut specimens with bigger grains.

According to the Vickers micro hardness test results, in UNS S32304 as-received samples, austenite is expected to be harder than ferrite. For UNS S32750 as-received samples, hardness of both phases are expected to be equivalent.
For after-tested UNS S32750 it has been observed qualitatively, through optical microscope imaging, that ferrite seems to be more ductile, while austenire tends to preserve its original shape.

The responsible for these differences are the different hardening mechanisms acting to austenite and ferrite; consequence of alloying element in the steel grade and thermomechanical history.

Due to their very good corrosion properties with respect to their mechanical ones and continuous improving of fabrication processes, duplex stainless steels are expected to be more used in the coming years as substitutes for ordinary carbon steels in many applications for weight-saving purposes.

8. Bibliographic references

[Alvarez-Armas, 2008] ALVAREZ-ARMAS, I. Duplex Stainless Steels: Brief History and Some Recent Alloys. **Recent Patents on Mechanical Engineering**, 2008, 1, 51-57.

[American Society for Metals, 1973] AMERICAN SOCIETY FOR METALS. **Metals Handbook**, 8th ed., vol. 8, p. 424. Metals Park, Ohio. 1973.

[ASM International, 1987] **ASM Handbook, Volume 13, "Corrosion"**, ISBN 0-87170-007-7, ASM International, 1987.

[ASM International, 1990] ***ASM handbook: Volume 1, Properties and selection: irons, steels, and high-performance alloys.*** Park, OH: ASM International. 1990

[ASM International, 1997] **Metals Handbook (Desk Edition) Chapter 32 (Failure Analysis),** ASM International, (1997) pp 32-24 to 32-26.

[ASM International, 2011] Editor: Reardon, A.C.. **Metallurgy for the Non-Metallurgist, Second Edition.** ASM International, 2011.

[ASTM E384] **ASTM E384-11e1, Standard Test Method for Knoop and Vickers Hardness of Materials,** ASTM International, West Conshohocken, PA, 2011.

[Bevitori, 2010] BEVITORI, A. **Influência da pré-deformação plástica na microestrutura e propriedades de um aço inoxidável superduplex**. Dissertação (Mestrado em Engenharia e Ciência dos Materiais). Universidade Estadual do Norte Fluminense Darcy Ribeiro. Centro de Ciência e Tecnologia. Laboratório de Materiais Avançados. Campos dos Goytacazes, 2010.

[Brandi, 1992] BRANDI, S.D. **Estudo da soldabilidade do aço inoxidável duplex DIN W. Nr. 1.4462(UNS S31803)**, Pg. 250. São Paulo, 1992.

[Callister, 2002] CALLISTER, W. D. Jr. ***Ciência e Engenharia de Materiais: Uma Introdução***, 5ª edição, editora LTC, *2002.*

[Charles, 2007] J.CHARLES. Duplex stainless steels, a review after dss '07 (Grado). Arcelor Mittal Stainless. (Review of the 100 scientific contributions presented during the **international duplex stainless steel conference** held in Grado). Italy, June 2007.

[Hirano, 2006] HIRANO, A.W. **Investigaçao da estrutura de deformação durante estricçao do aço inoxidável dúplex W.Nr 14462**. Trabalho de Conclusão de Curso, EPUSP, 2006.

[Hornbogen, 1984] HORNBOGEN, E. On the microstructure of alloys. **Acta Met**, 32(5):615-627, 1984.

[Jones, 1998] JONES, Rober M. Mechanics of Composite Materials. **(Materials Science & Engineering Series). Taylor & Francis Inc**; Edition: 2 Rev ed. (16. November 1998).

[Kenneth, 2012] KENNETH J. A., SHEN, C. , RAWLS, H.R. **Anusavice Phillip's Science of Dental Materials**. Saunders; 12 edition (October 11, 2012). ISBN: 9780721693873.

[Makinde, 1986] MAKINDE, A., FERRON, G. Modelling the Plastic Behaviour of Ductile and Anisotropic Two-Phase Materials with particular reference ti Duplex-phase Austenite- Ferrite Steels. **Materials Science and Engineering**, 83 (1986) 247-254.

[Moverare 2002] MOVERARE, J.J, ODÉN, M. Deformation behaviour of a prestrained duplex stainless steel. **Materials Science and Engineering** A337 (2002) 25-38.

[Nickel Development Institute, 2000] COVACH, Curtis W. **High performance stainless steels**. Nickel Development Institute. Toronto, Ontario M5H 3S6. Canada, 2000.

[Padilha and Plaut]. PADILHA, A., PLAUT, R., RIOS, P.R., In: Totten GE (editor). **Stainless steels heat treatment** (chapter 12). *Steel heat treatment handbook*. 2 ed. Boca Raton (FL, USA): CRC Press; 2007.

[Passchier and Trouw, 2005] PASSCHIER, C.W., TROUW, R.A., 2005. **Microtectonics**. **Springer**; 2nd edition, 2005. ISBN-10: 3540640037.

[Puttick 1958] PUTTICK, K.E., 1958. extracted from: Fracture. Edited by B. L. Averbach, D. K. Felbeck, G. T. Haiin and D. A. Thomas. **The Technology Press, Massachusetts Institute of Technology and John Wiley and Sons**, New York; Chapman & Hall Ltd., London, 1959.

[Renton 2006] RENTON, N. C., DEANS, W. F., BAKER, M. J. **Super-duplex stainless steel: a case study of incorporating anisotropic material properties into reliability assessments**. 3rd International ASRANet Colloquium. 10-12th July 2006, Glasgow, UK.

[Ruggieri, 2004] RUGGIERI, C. Numerical investigation of constraint effects on ductile fracture in tensile specimens. **J. Braz. Soc. Mech. Sci. & Eng**. vol.26 no.2 Rio de Janeiro Apr./June 2004. Dept. of Naval Architect. and Ocean Engineering University of São Paulo, SP. Brazil.

[Sandvik, 1994] FRODIGH, J., NICHOLLS J.M. **Mechanical Properties of Sandvik duplex stainless steels**. AB Sandvik Steel, S-811 81 Sandviken, Sweden. S-32-30-ENG. April 1994.

[Soboyejo, 2002] SOBOYEJO, W. Mechanical Properties of Engineered Materials **(Mechanical Engineering (Marcel Dekker)). CRC Press**; 1 edition (November 20, 2002).

[Vander 2004] VANDER, G.F. , VOORT, G.M. LUCAS, and E.P. MANILOVA, **Metallography and Microstructures of Stainless Steels and Maraging Steels,*Metallography and Microstructures,* Vol 9, *ASM Handbook,* ASM International**, 2004, p. 670-700.

[Zucato et al., 2002] ZUCATO, I., MOREIRA M.C., MACHADO I.F., S.M. LEBRAO. Microstructural Characterization and the Effect of Phase Transformations on Toughness of the UNS S31803 Duplex Stainless Steel Aged Treated at 850 °C. **Materials Research**, Vol. 5, No. 3, 385-389, 2002.

APPENDIX A

APPENDIX A - Sequences of cylindrical deformed sample after fracture

The following sequences complement the results and discussion of section 5.3. Metallography of after-tested specimens, more specific they can be used to observe some of the phenomena explained inside point 5.3.1. Cylindrical Specimen.

The sequences are zoomed parts (lighted in red and green in Figure 1 - Appendix). of the deformed cylindrical specimen.

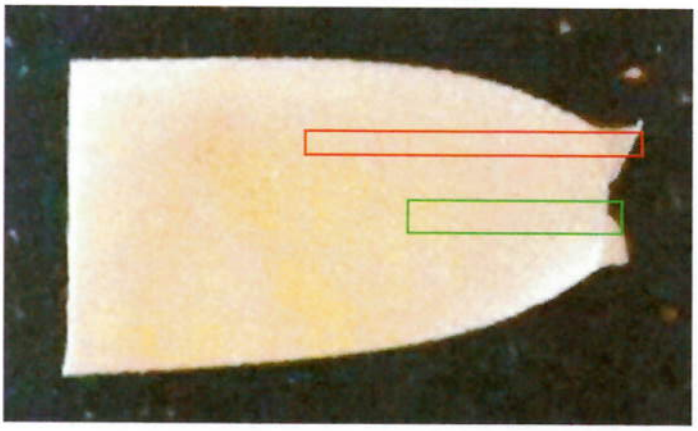

Figure 1 - APPENDIX. Zoom of Figure 26. Areas in the cylindrical fractured specimen that appear in the sequences. At the top, marked in red, area of sequence 1. At the bottom, marked in green, area of sequence 2.

A.1.1. Sequence 1 - Cylindrical deformed sample after fracture – Magnification 200x (Optical Microscope). Area of the sequence marked in red in Figure 1 - APPENDIX.

A.1.2. Sequence 2 - Cylindrical deformed sample after fracture – Magnification 100x (Optical Microscope). Area of the sequence marked in green in Figure 1 - APPENDIX

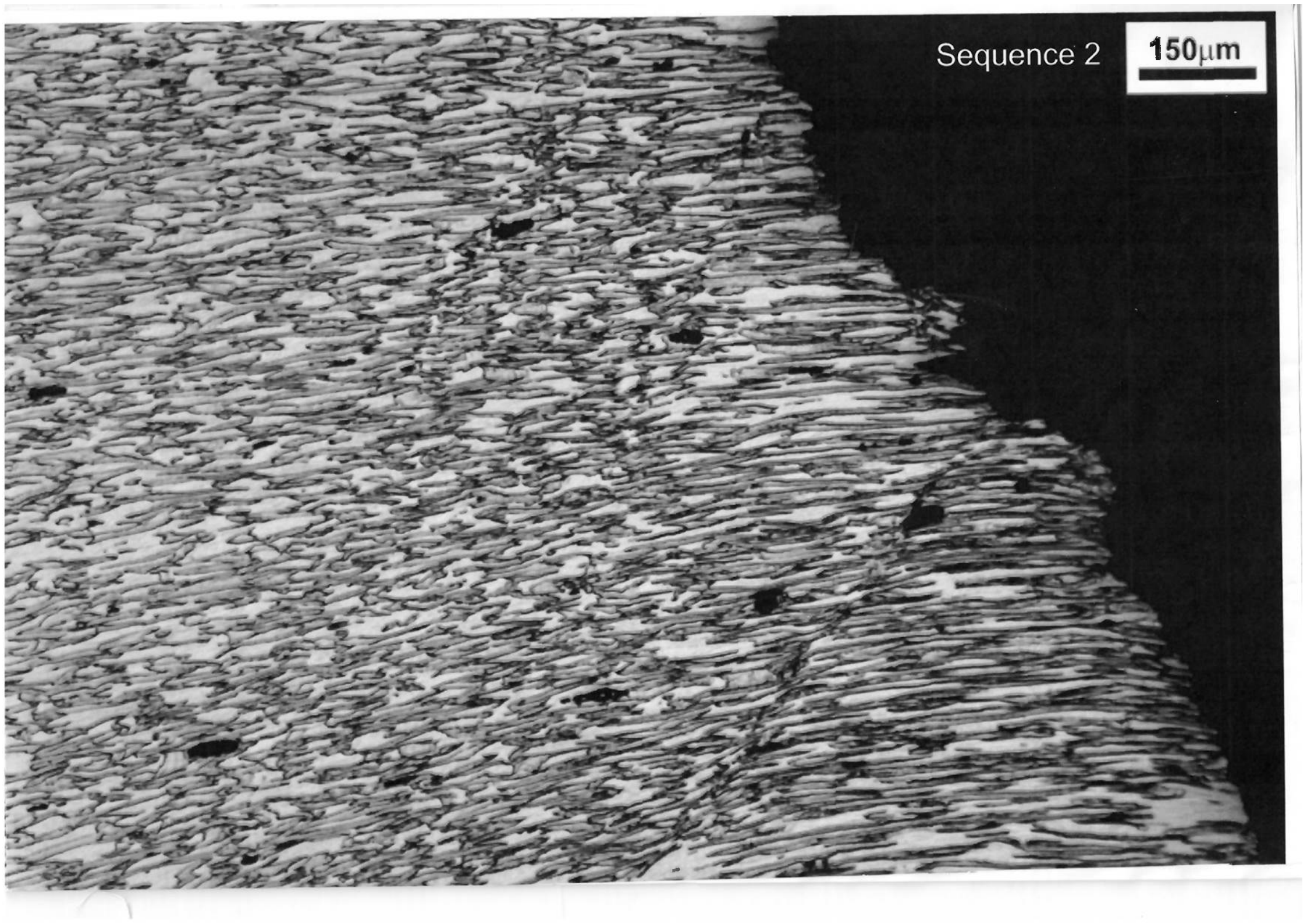
Sequence 2
150µm

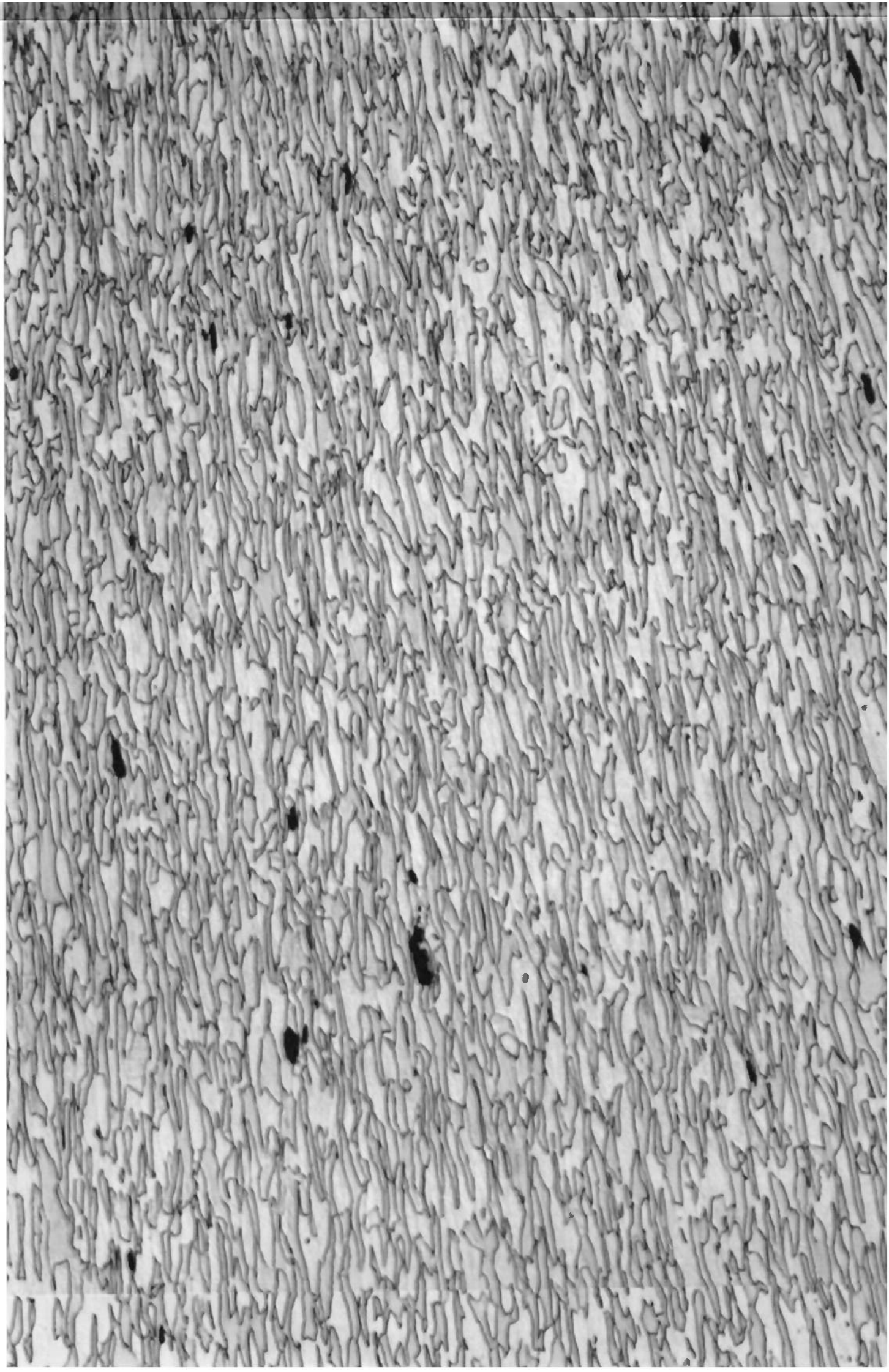

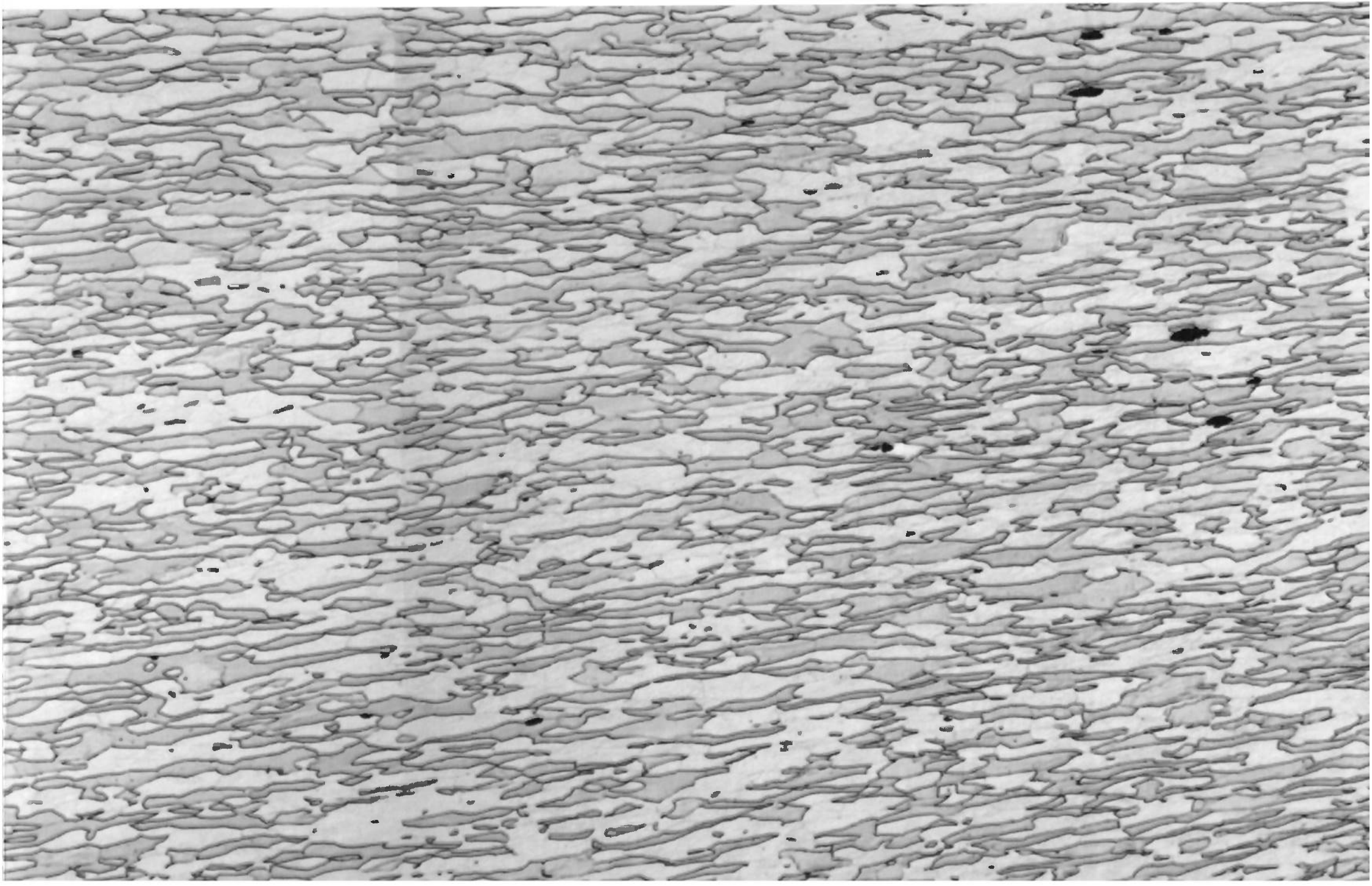

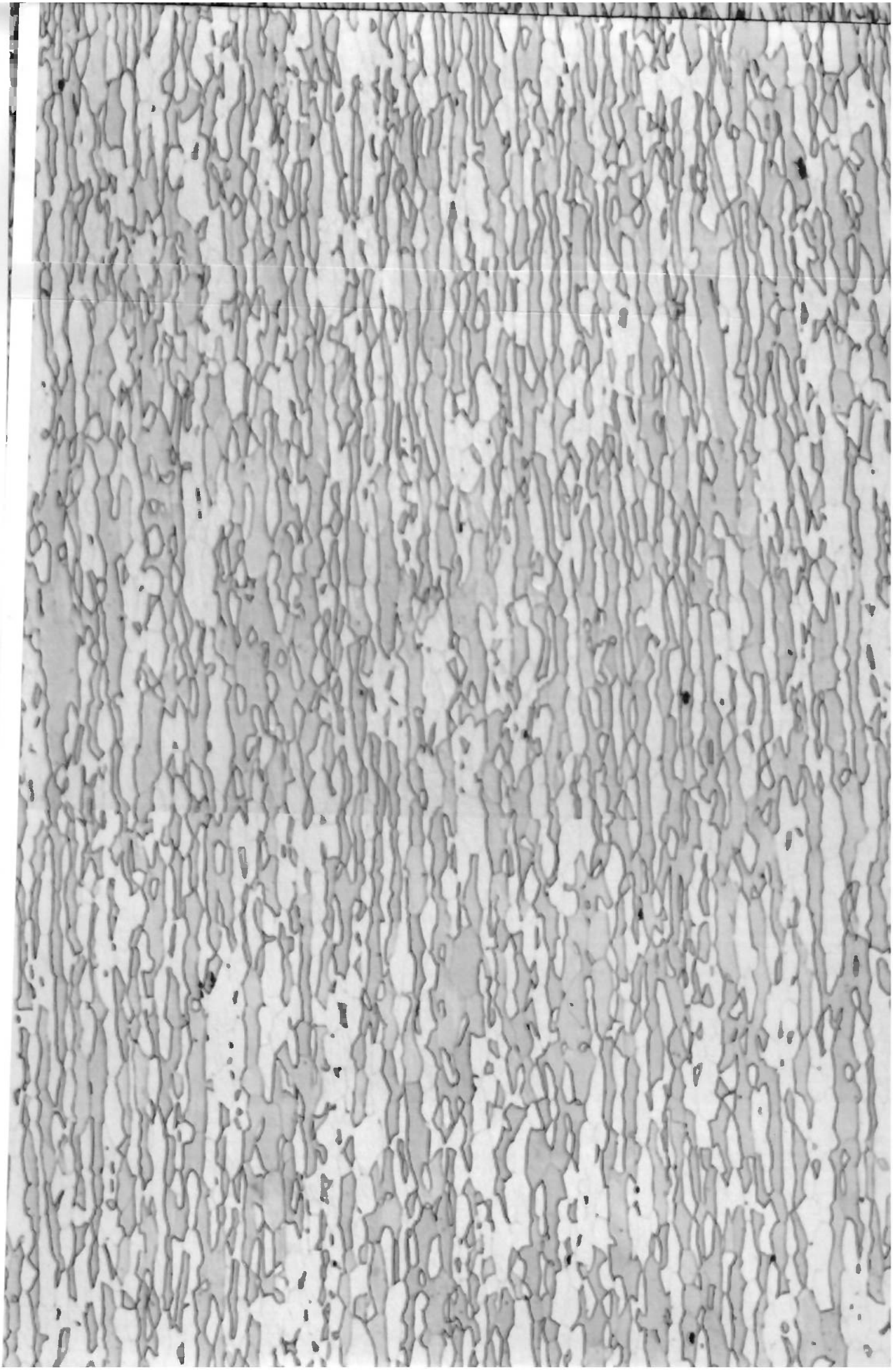

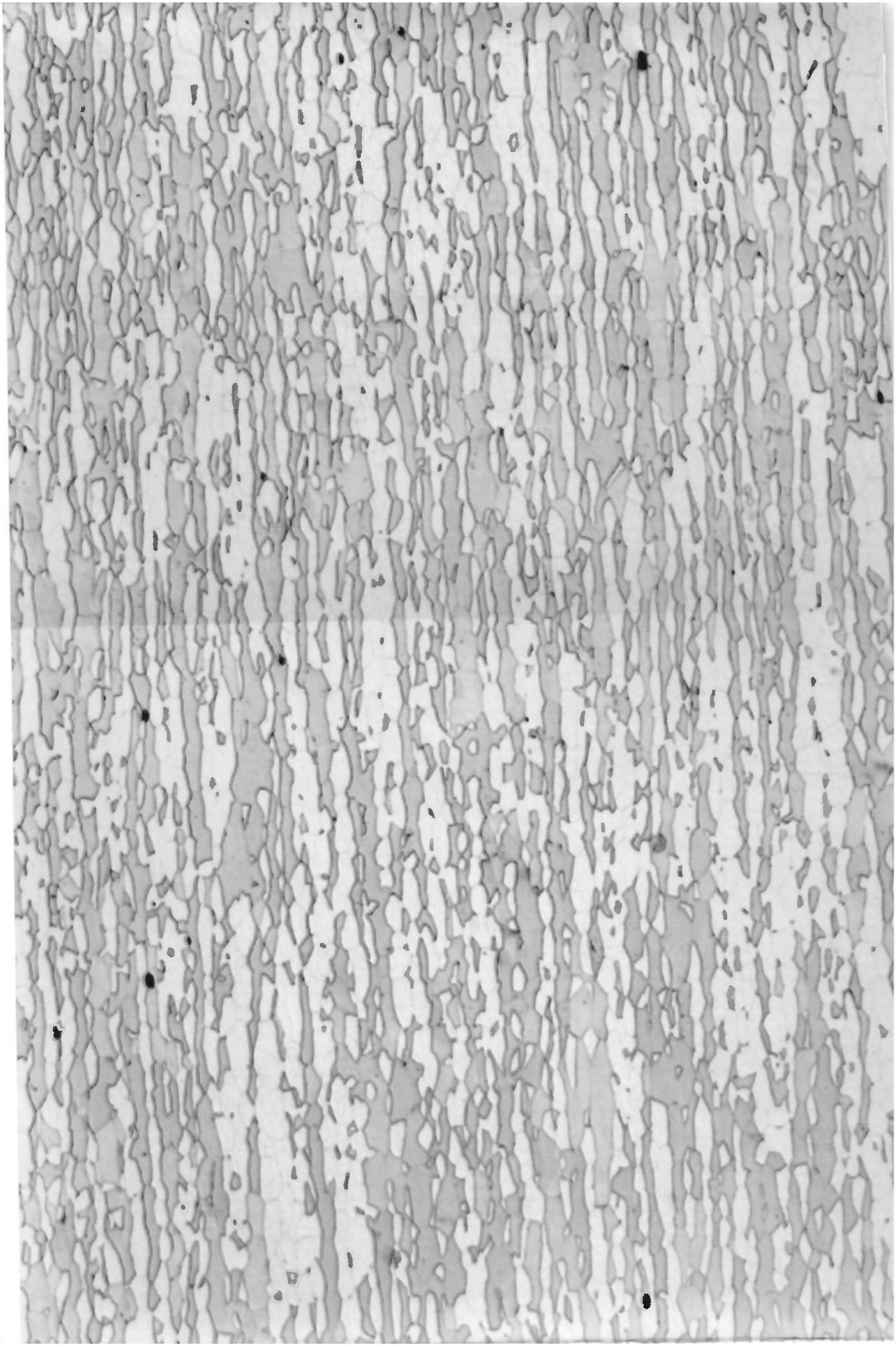

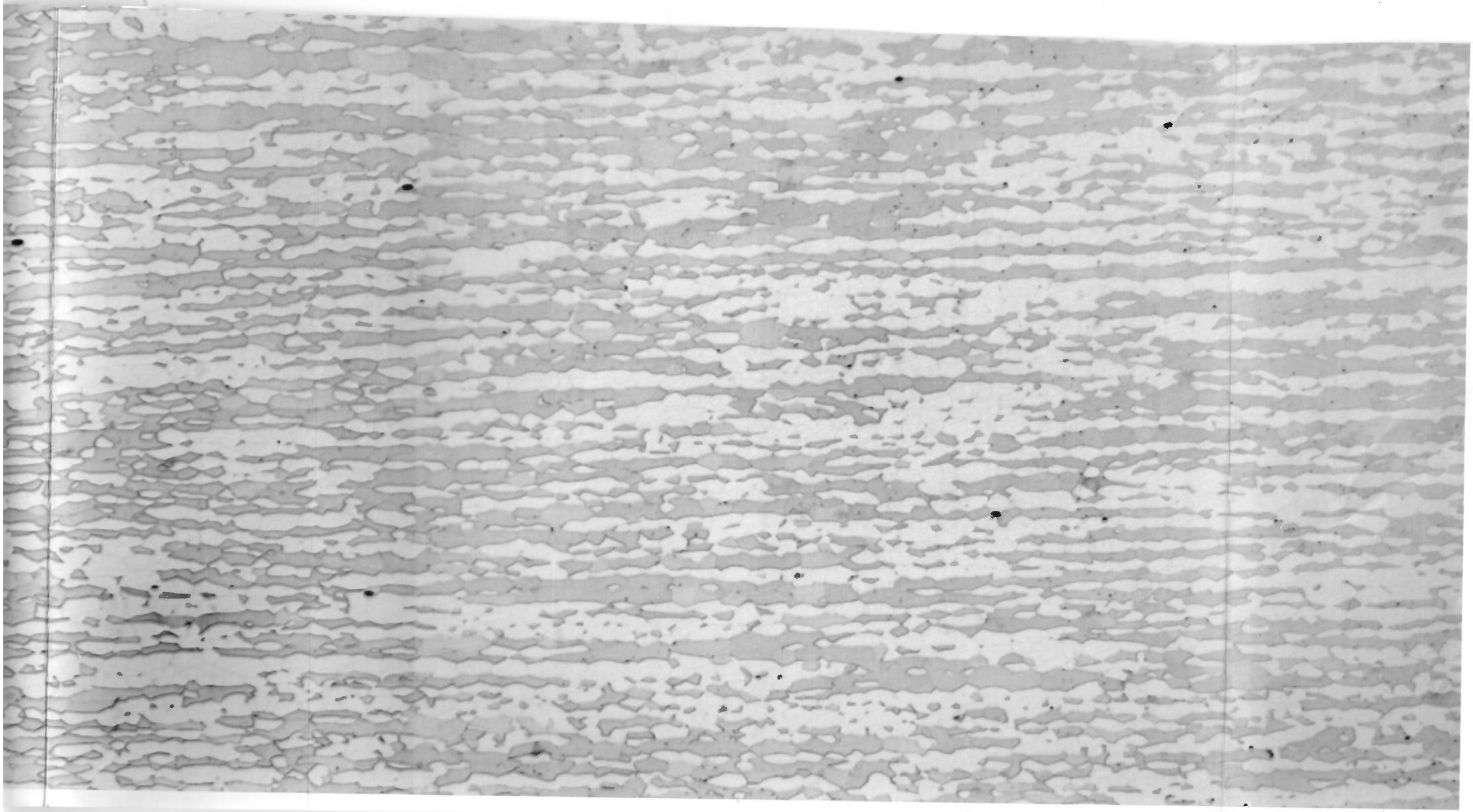

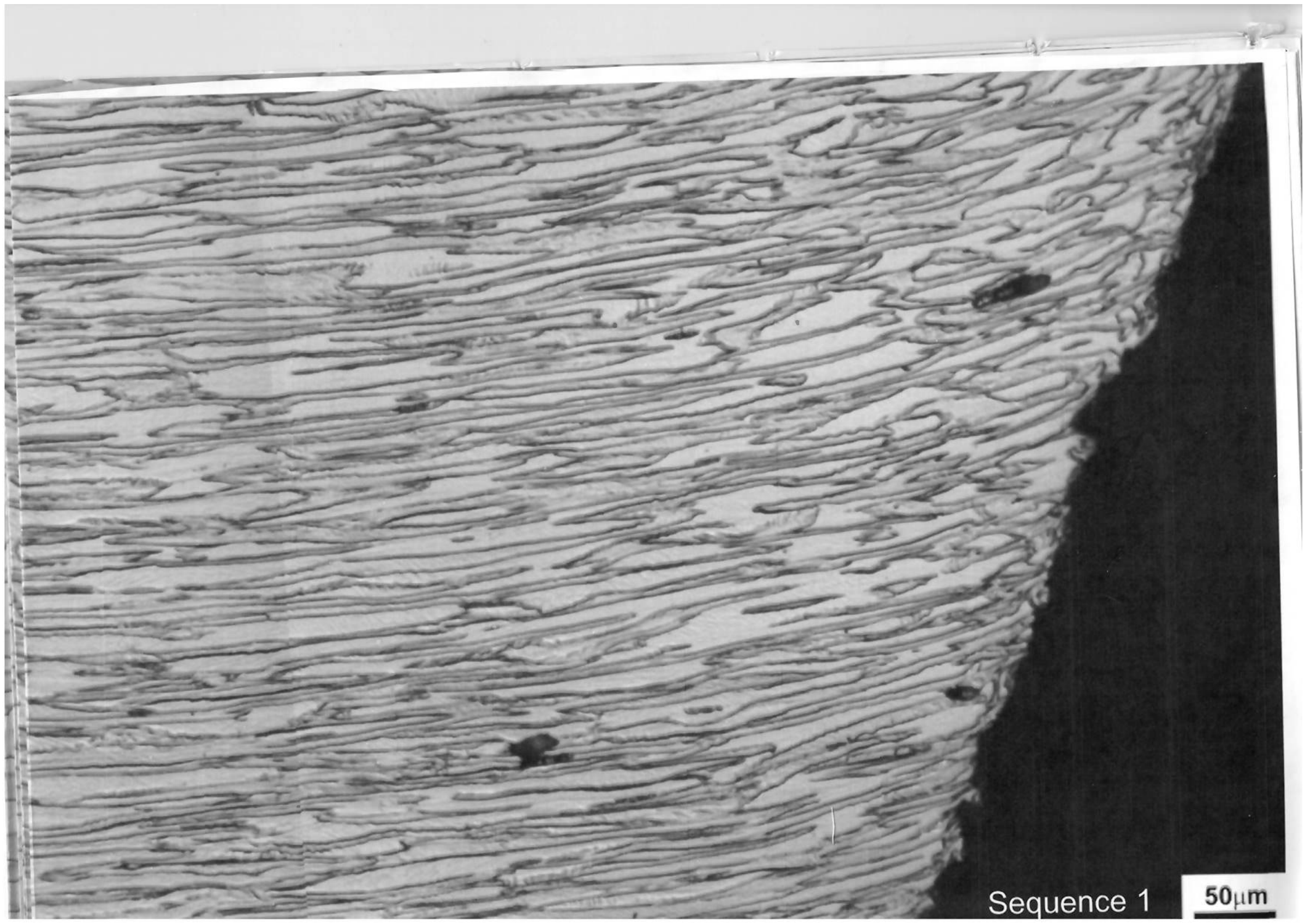
Sequence 1
50µm